remote sensing

MDPI

Article

The Divergent Changes in Surface Water Area after the South-to-North Water Diversion Project in China

Tongze Guo [1], Runkui Li [1,2,*], Zhen Xiao [1], Panli Cai [1], Jingxian Guo [1], Haiyu Fu [1], Xiaoping Zhang [1] and Xianfeng Song [1,2]

[1] College of Resources and Environment, University of Chinese Academy of Sciences, Beijing 100049, China; guotongze23@mails.ucas.ac.cn (T.G.); xiaozhen22@mails.ucas.ac.cn (Z.X.); caipanli19@mails.ucas.ac.cn (P.C.); guojingxian21@mails.ucas.ac.cn (J.G.); fuhaiyu22@mails.ucas.ac.cn (H.F.); zhangxp@ucas.ac.cn (X.Z.); xfsong@ucas.ac.cn (X.S.)

[2] State Key Laboratory of Resources and Environmental Information System, Institute of Geographic Sciences and Natural Resources Research, Chinese Academy of Sciences, Beijing 100101, China

* Correspondence: lirk@ucas.ac.cn

Abstract: Water scarcity is a significant challenge in China, and the South-to-North Water Diversion Project (SNWDP) aims to address the water deficit in the northern region. This study analyses Landsat 5/7/8 remote sensing imagery from 2001 to 2020 on the Google Earth Engine (GEE) cloud platform to assess the impact of the SNWDP on surface water bodies in water-receiving areas. Moreover, by integrating MODIS evapotranspiration data and ERA5 meteorological reanalysis data, this study comprehensively assesses the SNWDP's contribution to varied surface water body changes. Using an improved multi-temporal water frequency method, this study extracts max, seasonal, and year-long water surface areas. The results reveal that Beijing and Henan provinces have experienced significant increases in water surface areas post-SNWDP, with their max water surface area growing at a rate of 10.42 km^2/yr and 33.49 km^2/year, respectively. However, water surface areas in several provinces, especially those along the east route, were not observed to increase. The spatially detailed Mann–Kendall test indicates that the expansion of year-long water bodies is mostly concentrated near the central route project, revealing spatial heterogeneity in the water replenishment effect. Cropland and impervious surfaces are the main contributors to transfers in and out of water bodies. Meteorological and water use factors for spatial variations in water changes are also identified. These findings provide insights into the varied hydrological consequences of the SNWDP and contribute to the evaluation and management of similar large-scale water diversion projects around the world.

Keywords: water diversion; south-to-north water diversion project; long-term remote sensing; water body types; spatiotemporal change; Google Earth Engine

Citation: Guo, T.; Li, R.; Xiao, Z.; Cai, P.; Guo, J.; Fu, H.; Zhang, X.; Song, X. The Divergent Changes in Surface Water Area after the South-to-North Water Diversion Project in China. *Remote Sens.* **2024**, *16*, 378. https://doi.org/10.3390/rs16020378

Academic Editors: Monica Rivas Casado and Paraskevas Tsangaratos

Received: 18 October 2023
Revised: 8 December 2023
Accepted: 16 January 2024
Published: 17 January 2024

1. Introduction

Water security has persistently been a global challenge [1], and this issue is particularly pronounced in China, which is densely populated and rapidly urbanizing [2]. As the world's most populous nation with a highly uneven distribution of resources, China has long grappled with water scarcity and imbalanced water distribution [3,4]. According to relevant data, China's per capita water resources amount to a mere 2200 m^3/year, rendering extreme water scarcity a stark reality for the country [5]. In recent years, rapid urbanization and economic growth have intensified water demand, exacerbating water scarcity [6,7] and significantly aggravating China's water crisis. Conversely, China's water resources exhibit a spatial distribution pattern characterized by less water in the north and more in the south, with northern regions confronting water scarcity [8,9]. As the second largest plain in China, the North China Plain supports 25% of the nation's population but possesses only 3% of its freshwater resources, resulting in a severe water crisis in the region [10–13]. To address the water shortage in North China, the Chinese government has introduced a series

of policies and implemented various projects, with the South-to-North Water Diversion Project (SNWDP) being the most significant component.

The concept of the SNWDP originated in the 1950s, but it was not systematically planned until the 1990s, with construction commencing at the turn of the century. The project is regarded as a landmark in modern water conservancy engineering in China, aiming to resolve the water shortage in the northern region through water diversion and reallocation [14]. The SNWDP is a significant endeavour consisting of three water transfer routes—East, Central, and West—that cover a large portion of China. The East and Central routes began supplying water to the North in 2014. Since its implementation, the SNWDP has been instrumental in mobilizing water resources [15], delivering over 50 billion cubic metres of water to northern China. It has contributed to economic development in the recipient region [16,17], improved the ecological environment [18–21], and alleviated pressure on water resources [22,23]. Previous studies have highlighted the role of the SNWDP in stabilizing and replenishing groundwater resources [24–26]. However, most of these studies have primarily relied on gravity satellites and statistical data to assess the project's impact on land water storage, particularly groundwater, while overlooking changes in surface water. Surface water, as a crucial component of the terrestrial water cycle and water resources [27], holds significant importance for various aspects, such as human production, landscape ecology, and climate regulation [28–30]. Consequently, investigating the surface water variations in the SNWDP area is of significant importance for water resource protection and management.

Surface water body changes are influenced by a multitude of factors, including both natural and social factors [31,32]. Therefore, to accurately analyse the contribution of the SNWDP to surface water body changes, it is crucial to identify various factors simultaneously. For instance, meteorological factors like temperature and rainfall directly impact the formation and disappearance of surface water bodies, while human activities like urbanization and agricultural irrigation also have significant effects [33]. When assessing the SNWDP's impact, it is essential to comprehensively consider these factors and employ appropriate statistical methods to accurately evaluate the project's influence on surface water body changes. Additionally, it is important to acknowledge that surface water body changes can vary across different regions and time periods.

The SNWDP spans across Central and Northern China, where the industrial structure, economic conditions, intensity of human activities, and meteorological conditions exhibit significant spatial variations over different regions [34–38]. Furthermore, influenced by the resource management policies of various regions, the water usage patterns and resource management models vary with regional differences [39–41]. Additionally, due to the variations in water resource depletion and carrying capacity in each region [42,43], the SNWDP has differing effects on water resource restoration in various areas [44,45]. Therefore, a detailed assessment for each region is necessary to accurately address the impact of the SNWDP on surface water changes in different areas.

To identify the impact of the South-to-North Water Diversion Project on surface water changes in different regions, it is first necessary to accurately extract the spatiotemporal distribution of surface water bodies. The advancement of remote sensing earth observation technology and the availability of extensive data sources have led to increasingly widespread applications of surface water extraction [46,47]. Remote sensing, with its extensive monitoring range, archived data, and high timeliness, offers effective technical support for water ecological environmental protection and water resource development, and it has been applied in certain areas of the SNWDP [48,49]. Currently, the prevalent methods for water body extraction are primarily divided into two categories: threshold methods and classification methods [50,51]. Among the threshold methods, the water body index method is widely employed and has demonstrated effectiveness in extracting water bodies. Zou et al. [52] integrated the findings of previous studies and multiple indices to accurately extract long-term series water bodies in the United States, and this approach has been successfully applied in China [2,53]. Therefore, this study was carried out using this

widely adopted method and its optimized form to extract the spatiotemporal distribution of surface water bodies in the SNWDP areas.

In light of these considerations, this study aimed to improve the method for extracting the distribution of surface water bodies in the receiving areas of the SNWDP and analyse the divergent changes in water bodies before and after the recharge. Long-term multi-source remote sensing images and reanalysis data were utilized based on the Google Earth Engine (GEE) cloud computing platform. This study investigates the spatial and temporal changes of water bodies in the areas influenced by the SNWDP and identifies the driving factors behind these changes. It will provide a scientific basis for assessing, optimizing, and managing the effects of the SNWDP, and it can also support varied water transfer strategies according to local conditions. The findings of this study will contribute to the understanding of localized water resource management and provide a basis for the sustainable development of water-related projects.

2. Data and Methods

2.1. Study Area

The primary research area of this study includes the eastern and central routes of the SNWDP, which covers an expansive region of 1.05 million km^2 and encompasses 12 provinces and 94 cities (Figure 1). The eastern route originates from the Jiangdu Water Conservancy Hub in Yangzhou City, Jiangsu Province, while the central route begins at the Danjiangkou Reservoir, located in the middle and upper reaches of the Han River, a major tributary of Yangtze River. The SNWDP is an extensive undertaking, boasting over 3000 km of water conveyance infrastructure. It serves a population of nearly 400 million and spans multiple regions, including the North China Plain and the Huaihai Plain.

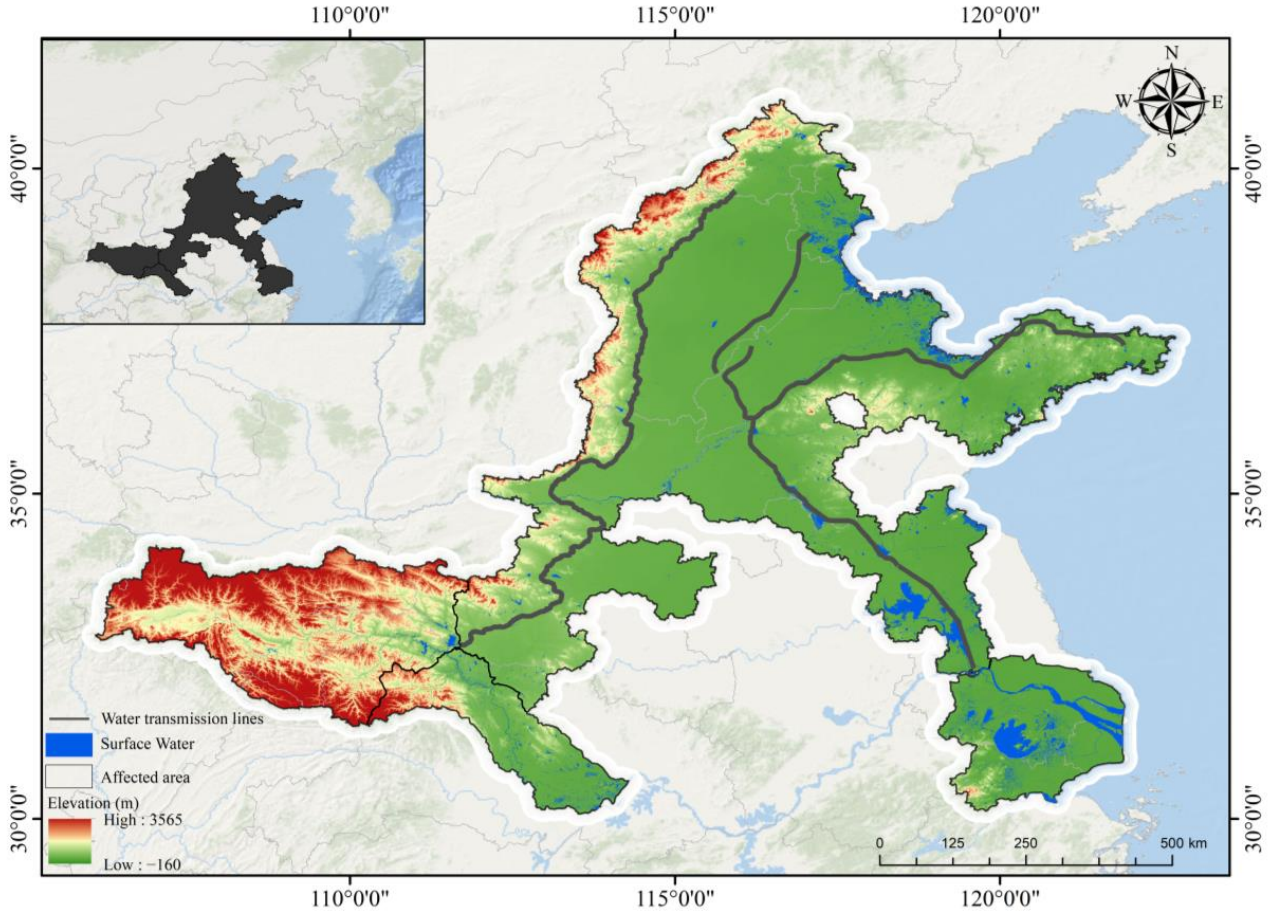

Figure 1. SNWDP routes and the influenced regions.

2.2. Research Data

This study primarily utilized seven categories of research data: meteorological data, evapotranspiration data, topographic and geomorphological data, remote sensing imagery, statistical data, land cover data, and fundamental geographic element data. The data were predominantly processed and extracted using the Google Earth Engine (GEE) platform, with some data being organized through ArcGIS.

(1) Meteorological data mainly include annual precipitation (AP) and 2 m height air temperature (Temp) derived from ERA5-Land reanalysis data [54]. These data have a spatial resolution of 0.1° × 0.1° and were analysed and extracted using the GEE platform. ERA5 data have been proven to accurately represent the interannual and seasonal characteristics of precipitation in China, making these data suitable for practical studies [55,56].

(2) Evapotranspiration data primarily consist of MODIS evapotranspiration (ET) data, which have a spatial resolution of 500 m × 500 m [57].

(3) Topographic and geomorphological data are mainly derived from ALOS Earth observation DEM data [58], and these data have a spatial resolution of 30 m × 30 m.

(4) Remote sensing images were obtained from the Landsat series of Earth observation satellites. All series of Landsat satellite images (5/7/8) of the South-to-North Water Diversion region from 2001 to 2020 were acquired using the GEE platform. The Landsat-5/7/8 images are courtesy of the U.S. Geological Survey. To ensure higher-quality images, this study employed the de-clouding algorithm CFMask to remove clouds, cloud shadows, and snow, resulting in a collection of high-quality images. A total of 10,321 Landsat satellite images were used to extract water bodies within the research area (Figure 2).

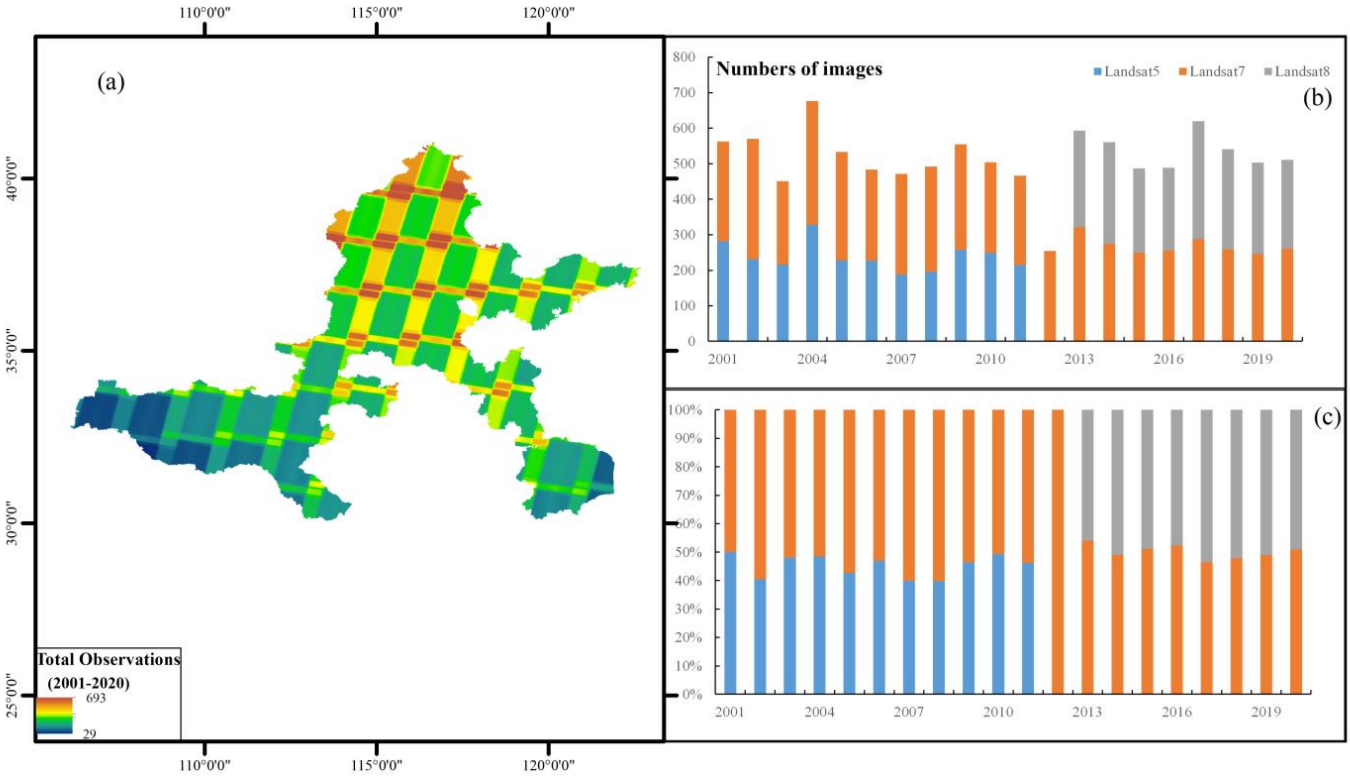

Figure 2. The distribution of Landsat 5, 7, 8 images for the SNWDP regions: (**a**) the total number of Landsat observations; (**b**) the total number of images from different Landsat sensors; (**c**) the proportion of different Landsat sensors in each year.

(5) The compendium of statistical data primarily encompasses information pertaining to the volumetric transference of water facilitated by the SNWDP across various provinces and municipalities. Additionally, it incorporates data on the consumption of water in each respective province and city, and these data are further sorted into the following categories: agricultural water consumption (Agcwu), industrial water consumption (Idswu), and the consumption of non-service public water use (Cnspwu). The aforementioned data were meticulously extracted from the bulletins of provincial and municipal water resources.

(6) Land cover data. The China land cover data (CLCD) used in this study were developed by Huang and Yang [59]. This dataset, with its 30 m resolution, boasts an overall accuracy of 80%, thereby outperforming other notable datasets such as MCD12Q1, ESACCI_LC, FROM_GLC, and GlobeLand30. For the purpose of this study, land cover data from the years 2013 and 2020 were harnessed to scrutinize the significant metamorphoses of aquatic body types within the geographical confines of the SNWDP.

(7) Fundamental geographic element data, including Chinese provincial and municipal administrative boundaries, were sourced from the 1:1 million Chinese Basic Geographic Information Database of the National Basic Geographic Information Center.

Using the GEE cloud computing platform, a comprehensive dataset for assessing surface water frequency, temperature, precipitation, and evapotranspiration in the research area from 2001 to 2020 was obtained through calculations.

2.3. Research Method

2.3.1. Water Body Extraction Method and Improvements

In this study, the waterbody extraction algorithm devised by Zou et al. [60] was utilized and enhanced to identify the distribution of waterbodies within the South-to-North Water Diversion Project's zone of influence. The algorithm relies on the relationship between water body indices and vegetation indices for feature discrimination. Specifically, three indices were employed: the Modified Normalized Difference Water Body Index $(mNDWI)$, the Normalized Difference Vegetation Index $(NDVI)$, and the Enhanced Vegetation Index (EVI). The calculations for these three indices are as follows:

$$mNDWI = \frac{\rho_{Green} - \rho_{SWIRI}}{\rho_{Green} + \rho_{SWIRI}} \tag{1}$$

$$NDVI = \frac{\rho_{NIR} - \rho_{Red}}{\rho_{NIR} + \rho_{Red}} \tag{2}$$

$$EVI = 2.5 \times \frac{\rho_{NIR} - \rho_{Red}}{1.0 + \rho_{NIR} + 6.0\rho_{Red} + 7.5\rho_{Blue}} \tag{3}$$

where ρ_{Green} represents the green band reflectance, ρ_{Red} denotes the red band reflectance, ρ_{Blue} signifies the blue band reflectance, ρ_{SWIRI} corresponds to the short-wave infrared band reflectance, and ρ_{NIR} refers to the near-infrared band reflectance. Ultimately, the water body discrimination algorithm, which incorporates the aforementioned indices, is as follows:

$$water = (EVI < 0.1)\ and\ (mNDWI > EVI\ or\ mNDWI > NDVI) \tag{4}$$

If the EVI value is below 0.1 and $mNDWI$ exceeds either EVI or $NDVI$, the feature is identified as a water body. Building upon this, after classifying multiple images of the same area within a year, the annual frequency of water body occurrences is calculated cumulatively. The frequency of water bodies is determined using the following formula:

$$F(y) = \frac{1}{N_y} \sum_{i=1}^{N_y} W_{y,i} \tag{5}$$

where $F(y)$ is the water frequency, a measure of the occurrence of water that ranges from a minimum value of 0 to a max value of 1; y is the year; N_y is the total number of observations in a year for a certain image element; $W_{y,i}$ represents whether the image element is discriminated as a water body at the ith observation in the yth year (1 if it is a water body; 0 otherwise). The figure below shows a flow chart of the algorithm's entire process.

In mountainous areas, there is a situation where water bodies are mistakenly identified as shadows of the mountains. Therefore, Zou et al. [52] used DEM data to calculate mountain shadows and improved the accuracy of water body identification. In this study, we used ALOS AW3D30 data to identify mountain shadows and remove their impacts on water body extraction. In practical situations, the shadows cast by buildings in urban areas can also be classified as water, thus affecting the accuracy of water body extraction, which has lacked consideration in previous algorithms. Particularly in the SNDWP's region of influence, there are a large number of dense buildings, which can introduce errors in the extracted surface water bodies. To address this challenge, we integrated the global impervious surface data published by Gong et al. [61] to mask out building shadows, resulting in more accurate water body frequency data (Figure 3).

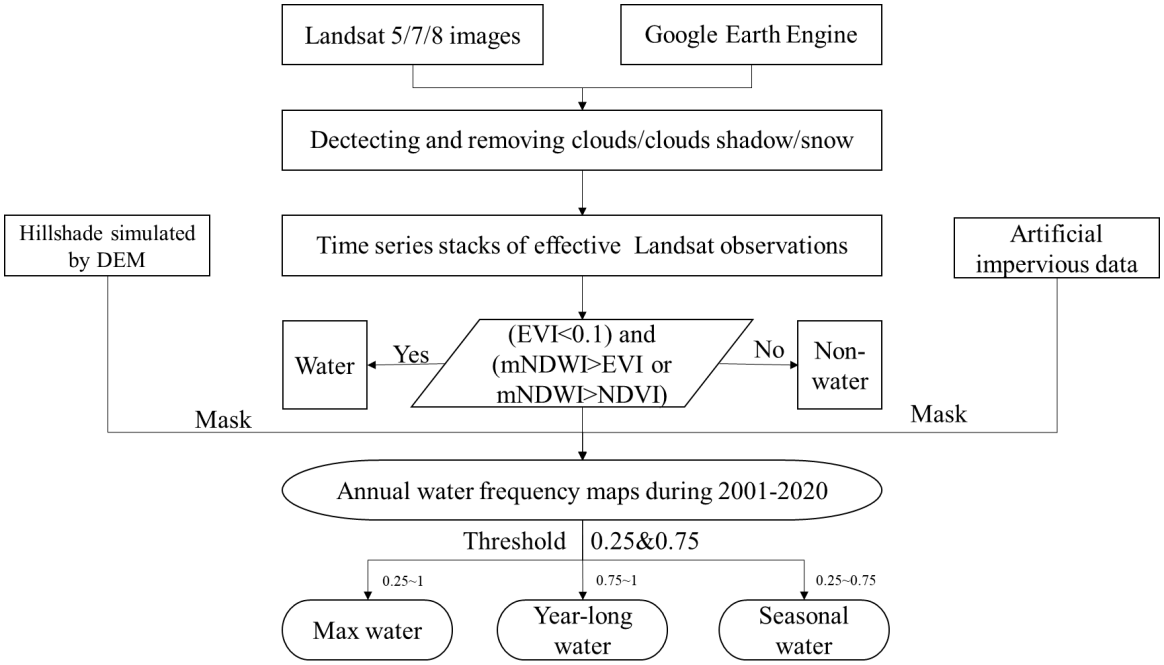

Figure 3. Flow chart for the extraction of different types of water bodies.

In this study, the integration of DEM data and impervious surface data effectively reduced significant noise from the water frequency data. However, some image misclassifications and omissions still remained. To address data-related issues and algorithm recognition errors, we implemented reasonable thresholds based on prior studies [52,60,62]. Specifically, we set the water body frequency threshold at 0.25 to minimize these impacts. Additionally, we categorized the water frequency threshold into three main classifications: seasonal water bodies (water frequency between 0.25 and 0.75), year-long water bodies (water frequency between 0.75 and 1), and max water bodies (water frequency between 0.25 and 1, the union of seasonal water body and max water body). This classification method enabled us to determine the annual distribution of seasonal, year-long, and max water bodies within the regions influenced by the SNWDP.

2.3.2. Spatial and Temporal Change Analysis

The South–North Water Diversion Project's central line and the east line were completed and first connected in 2014, marking a significant milestone. In order to analyse the

impact of the SNWDP, we designated 2014 as the SNWDP reference point and conducted linear regression analyses on the water body areas before and after this year. This approach allowed us to observe the change trends for before and after the implementation of the SNWDP, and we also used the following equation to do this:

$$y_i = k_i x + b_i \tag{6}$$

where y_i is the area of the water body in the ith region, k_i is the slope of the ith region, and x is the year. In this study, we set 2014 as the breakpoint year and conducted segmented linear regression before and after the breakpoint year to observe the change trends regarding the surface water body areas in each region before and after the SNWDP.

In order to further investigate the spatial variation in the water body areas and the spatial and temporal changes in rainfall and evapotranspiration from a spatial perspective, the Mann–Kendall test [63] and Theil–Sen Median method [64] were employed to examine spatial variations on different raster scales. The Theil–Sen Median is commonly used to estimate the average rate of change and trend in time series, and in this study, it was utilized to calculate the slope β of the time series data. For time series data $X_i = (x_1, x_2, \ldots, x_3)$, it can be expressed by the formula:

$$\beta = Median\left(\frac{x_j - x_i}{j - i}\right), \forall j > i \tag{7}$$

where *Median* is the median function. If $\beta > 0$, it indicates an upward trend in the time series data, while if $\beta < 0$, it suggests a downward trend.

The Mann–Kendall test is a widely used technique for trend analysis in environmental data series. It is particularly effective in detecting monotonic trend changes and identifying potential turning points in time series data. The calculation process involves determining the relationship between the magnitudes of x_i and x_j for all pairs of values (represented as S) for a set of time series data $X_i = (x_1, x_2, \ldots, x_n)$. The test is based on two assumptions: (1) H_0: the data in the series are randomly arranged, indicating no significant trend; (2) H_1: there exists an upward or downward monotonic trend in the series. The test statistic S is calculated as follows:

$$S = \sum_{i=1}^{n-1} \sum_{j=i+1}^{n} sgn(x_j - x_i) \tag{8}$$

$$sgn(x_j - x_i) = \begin{cases} +1, x_j - x_i > 0 \\ 0, x_j - x_i = 0 \\ -1, x_j - x_i < 0 \end{cases} \tag{9}$$

where the selection of the significance test statistic depends on the length of the time series, denoted as n. When $n < 10$, the statistic S is directly used for the two-sided trend test. At a given significance level α, if $|S| \geq S_{\alpha/2}$, then H_0 is rejected, indicating a significant trend in the original series. Conversely, if $|S| < S_{\alpha/2}$, H_0 is accepted and the series is considered to have an insignificant trend. If $S > 0$, the series is considered to have an upward trend. If $S = 0$, there is no trend, and if $S < 0$, a downward trend is considered to exist. When $n \geq 10$, the statistic S approximately follows a standard normal distribution, and the trend test is performed using the test statistic Z. The formula for calculating the value of Z is as follows:

$$Z = \begin{cases} \frac{S-1}{\sqrt{VAR(S)}}, S > 0 \\ 0, S = 0 \\ \frac{S+1}{\sqrt{VAR(S)}}, S < 0 \end{cases} \tag{10}$$

where $VAR(S) = (n(n-1)(2n+5) - \sum_{i=1}^{m} t_i(t_i-1)(2t_i+5))/18$; n is the number of data points in the time series; m represents the number of knots (recurring datasets) in the series; t_i is the width of the knot (the number of repeated data in the ith set of repeated datasets). For the trend test, a two-sided approach is adopted. The critical value $Z_{1-\alpha/2}$ is checked

in the normal distribution table at a given significance level α. When $|Z| \leq Z_{1-\alpha/2}$, the original hypothesis was accepted and the trend was not significant; if $|Z| > Z_{1-\alpha/2}$, the original hypothesis was rejected and the trend was considered significant.

To examine the spatial and temporal variation characteristics of each parameter on a larger scale, this study utilized the aggregation tool to consolidate data on water bodies, ET, AP, and Temp into percentage data at a $0.5^\circ \times 0.5^\circ$ spatial unit. Moreover, to capture more detailed trends in surface water bodies, the water body data were further aggregated into percentage data with a 1 km $\times$ 1 km scale to examine the spatial and temporal dynamics of the surface water changes across the different regions.

2.3.3. Quantify the Impacts of the SNWDP on the Water-Receiving Areas

In order to characterize the recharge intensity of the water-receiving areas of the South-to-North Water Diversion Project, two indices are proposed in this study: recharge water intensity (*RWI*) and recharge surface water intensity (*RSWI*).

$$RWI = \frac{\text{Received water volume}}{\text{Total Area}} \tag{11}$$

$$RSWI = \frac{\text{Received water volume}}{\text{Max water area}} \tag{12}$$

where Received water volume denotes the amount of water transferred by the SNWDP in the year for the region, Total Area denotes the total area of the region (including non-water areas), and Max water area denotes the maximum water body area of the region in the previous year, which does not include non-water areas. By using the above two equations, we calculated the *RWI* and *RSWI* of each water-receiving area of the SNWDP to represent the recharge intensity through the project.

To examine the effect of the SNWDP on water bodies in the receiving areas, linear regression analyses were conducted to explore the role of different factors on the area of different water bodies. These factors mainly include Agcwu, Idswu, Cnspwu, ET, AP, Temp, and SNWDP water transfer volume. In addition, a land transfer matrix based on CLCD data was used in this study to explore the major changing traces of water bodies. Finally, to assess the impact of the SNWDP on changes in surface water area, correlation analysis was employed.

3. Results

3.1. Assessment of the Accuracy of Water Body Extraction

We selected four classic cities in the North China Plain, all are situated near the central route of the South-to-North Water Diversion Project, are characterized by high building density, and have been significantly impacted by the project (Figure 4). The figure reveals that the pre-improvement original algorithm in these areas mistakenly identified numerous building shadows as water bodies. In contrast, our improved algorithm effectively mitigates errors due to building shadows and efficiently extracts the spatial distribution of surface water bodies, thus proving the algorithm's enhanced applicability in areas with densely populated human settlements.

In this study, the extraction of max, year-long, and seasonal water bodies was conducted by utilizing consistent imagery and methodologies to ensure comparability in terms of classification accuracy. Year-long water bodies were used as the reference for our accuracy assessment. Visual interpretation techniques were employed to distinguish genuine water body image elements from non-water body image elements in the remote sensing imagery. The accuracy of the extracted water bodies was then evaluated using a confusion matrix.

Table 1 shows the accuracy results for year-long water bodies, with a user accuracy of 94.04%, a producer accuracy of 97.54%, and an overall accuracy of 96.16%. The Kappa coefficient, which measures agreement beyond chance, is 0.95, indicating that the algo-

rithm used to ensure the classification accuracy of the water bodies in this study yields superior outcomes and precisely delineates the distribution of water bodies within the area influenced by the SNWDP.

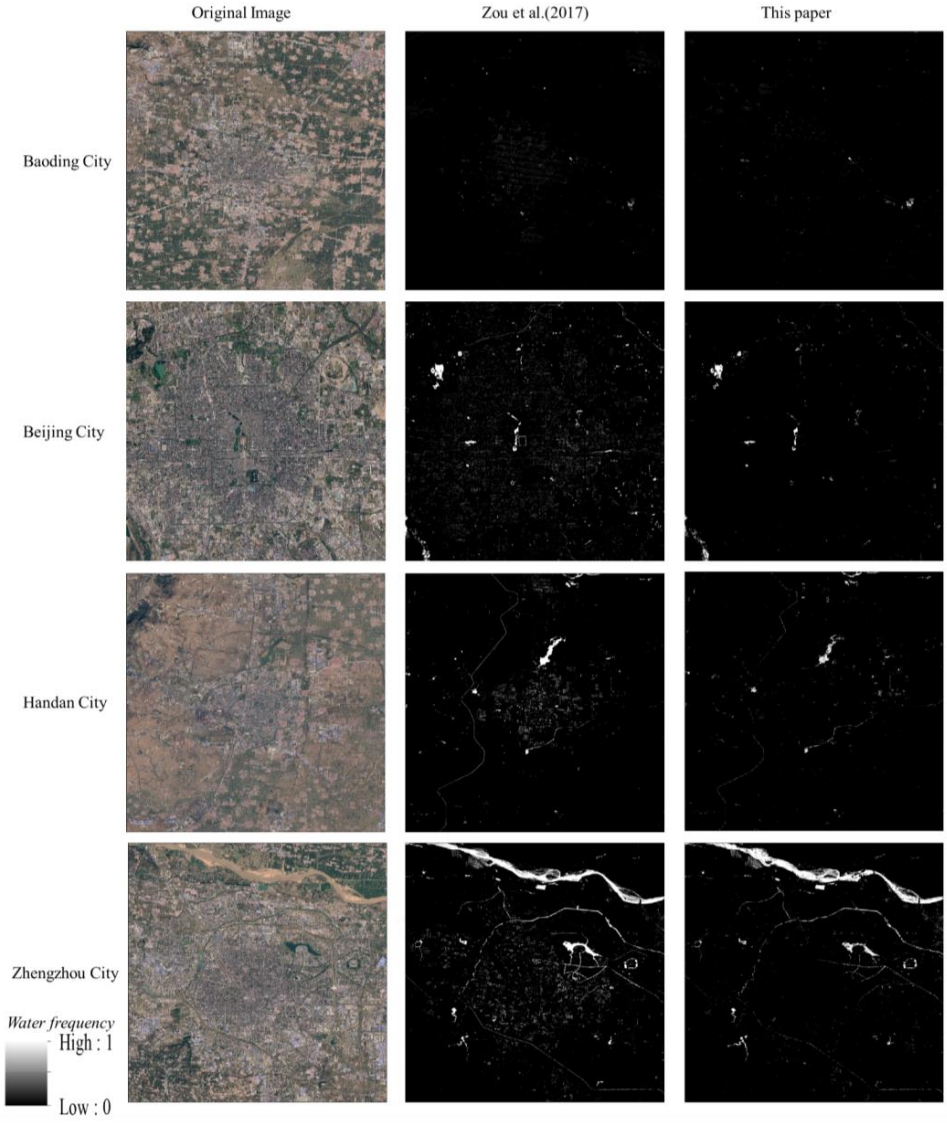

Figure 4. Comparison of water body extraction methods in high-density built-up areas (Zou et al., 2017 [52]).

Table 1. Confusion matrix of water body classification results based on Landsat 5/7/8 images.

Classification (2020)	Water	Non-Water	Total	User Accuracy (%)
Water	915	58	973	94.04
Non-water	23	1116	1139	97.98
Total	938	1174		OA = 96.16
Producer accuracy (%)	97.54	95.06		Kappa = 0.95

3.2. Changes in a Specific Water Body in a Typical Area

Due to the significant impact of the SNWDP, the Miyun Reservoir—the northernmost receiving area—was chosen as a representative region in this study to examine changes in its water body area. Constructed in the 1960s, the Miyun Reservoir has been a crucial water source for Beijing. However, factors such as climate change and rapid urbanization

have resulted in a decline in the reservoir's water storage capacity, leading to severe water shortages in Beijing.

As shown in Figure 5, the max water body area of the Miyun Reservoir showed a decreasing trend before 2014. However, after 2014, the max water body area of the Miyun Reservoir showed a significant increasing trend ($p < 0.01$). Specifically, from 2001 to 2004, the max water body area of the Miyun Reservoir continued to decrease, became stable from 2005 to 2014, and then rapidly increased after 2014.

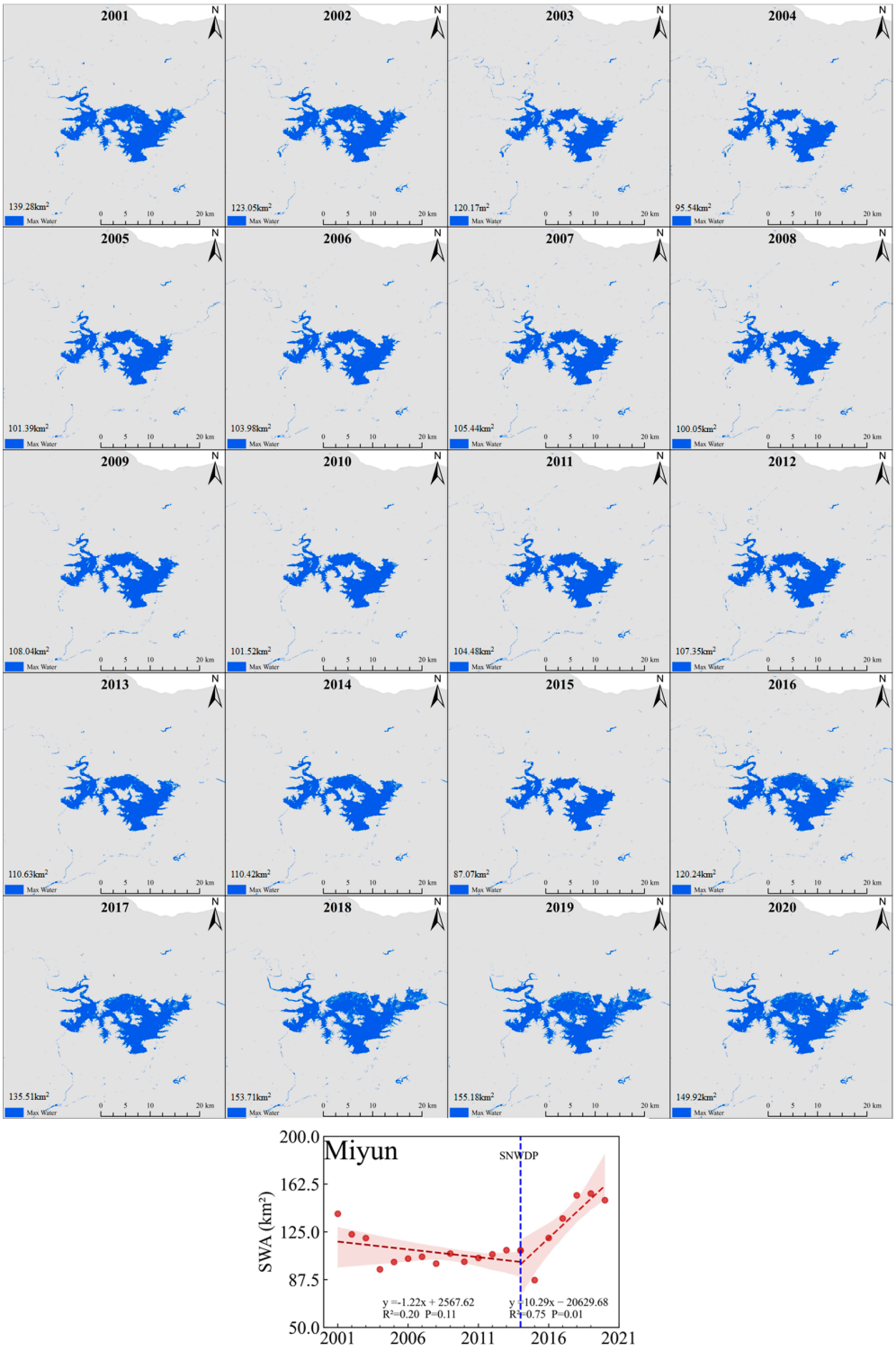

Figure 5. Changes in max water body area in the Miyun Reservoir.

Furthermore, it is crucial to recognize that changes in surface water bodies are influenced not only by the SNWDP but also by meteorological factors and human activities. While remote sensing images reveal a trend in water body changes consistent with the impact of the project, it is necessary to delve into later sections to discuss the specific and detailed effects of the project on surface water bodies.

3.3. Temporal Trends

3.3.1. Trends in Max Water Body

Figure 6 shows the change trend regarding the max water bodies in the regions influenced by the SNWDP. As the SNWDP's east and central routes commenced operations in 2014, this year was selected as the starting point at which we began evaluating the SNWDP's impacts. Trends before and after 2014 were analysed separately. Our findings reveal that, except for Hebei Province, the max water body area in the other regions exhibited a decreasing trend prior to 2014. Specifically, Jiangsu Province (62.59 km^2/year, R^2 = 0.46, p = 0.01), Henan Province (10.20 km^2/year, R^2 = 0.43, p = 0.02), Shandong Province (27.11 km^2/year, R^2= 0.60, p = 0.01), Shanghai City (4.61 km^2/year, R^2 = 0.65, p = 0.01), and Tianjin City (33.14 km^2/year, R^2 = 0.41, p = 0.01) all experienced a significant decreasing trend. Interestingly, after the first water connection, most of these regions experienced a reversal in their declining trends. Notably, Henan Province (33.49 km^2/year, R^2 = 0.56, p = 0.05) and Beijing City (10.42 km^2/year, R^2 = 0.68, p = 0.02) displayed the most significant increases in water body area. Although Jiangsu Province, Hubei Province, Shandong Province, and Tianjin City did not exhibit significant increases, they did deviate from their original continuous declining trends. Hebei Province initially showed a significant increasing trend until 2014 (19.03 km^2/year, R^2 = 0.60, p = 0.01), but after 2014, it changed its original trend. In contrast, the max water body area in Zhejiang Province displayed a relatively smooth change, without a clear trend. Overall, the most significant increases in the max water body area were observed in Henan Province and Beijing after 2014.

3.3.2. Trends in Year-Long Water Body

Based on Figure 7, the year-long water body changes in different regions exhibited various trends. Prior to 2014, some regions had a decreasing trend in their water body area, such as the total region, Jiangsu Province, Shanghai City, and Tianjin City. Specifically, the total region initially showed a short-lived increasing trend between 2001 and 2004 but later displayed a significant decreasing trend (77.47 km^2/year, R^2 = 0.47, p = 0.01). Similarly, Shanghai City (1.63 km^2/year, R^2 = 0.27, p = 0.06) and Tianjin City (21.63 km^2/year, R^2 = 0.44, p = 0.01) also showed a decreasing trend. However, after 2014, the trends of these regions changed and they started exhibiting an increasing trend, except for Shanghai City, which continued to show a decreasing trend. The increasing trend became more significant and obvious in Henan Province and Beijing City. The year-long water body areas in Zhejiang Province and Hubei Province were more variable, making it difficult to observe clear changes after the implementation of the SNWDP. Overall, based on evaluating the change trends and their significance, the most significant changes were observed in Henan Province and Beijing, both of which showed significant increases after 2014.

3.3.3. Trends in Seasonal Water Body

Based on Figure 8, the change trend regarding seasonal water bodies is more similar to that of the max water bodies. Until 2014, most regions (except Hebei Province and Zhejiang Province) showed a decreasing trend in their seasonal water body areas. Specifically, the total region showed a significant decreasing trend (122.07 km^2/year, R^2 = 0.43, p = 0.01), along with Hubei Province (18.43 km^2/year, R^2 = 0.23, p = 0.08), Shandong (68.71 km^2/year, R^2 = 0.57, p = 0.01), Shanghai city (2.97 km^2/year, R^2 = 0.56, p = 0.01), and Tianjin city (11.51 km^2/year, R^2 = 0.21, p = 0.10). However, after 2014, the total region, Jiangsu Province, Hubei Province, and Shandong Province exhibited an increasing trend in their seasonal water body areas. Notably, Shandong Province showed a significant increasing trend

(22.17 km^2/year, R^2 = 0.56, p = 0.05). The change trend for Hebei Province was different from that of the other regions. It showed a significant increasing trend until 2014 (10.65 km^2/year, R^2 = 0.56, p = 0.05) but no longer exhibited an increasing trend after 2014. In summary, based on the evaluating change trends and their significance, the most pronounced change in seasonal water bodies was observed in Shandong Province, which showed a significant increase after 2014.

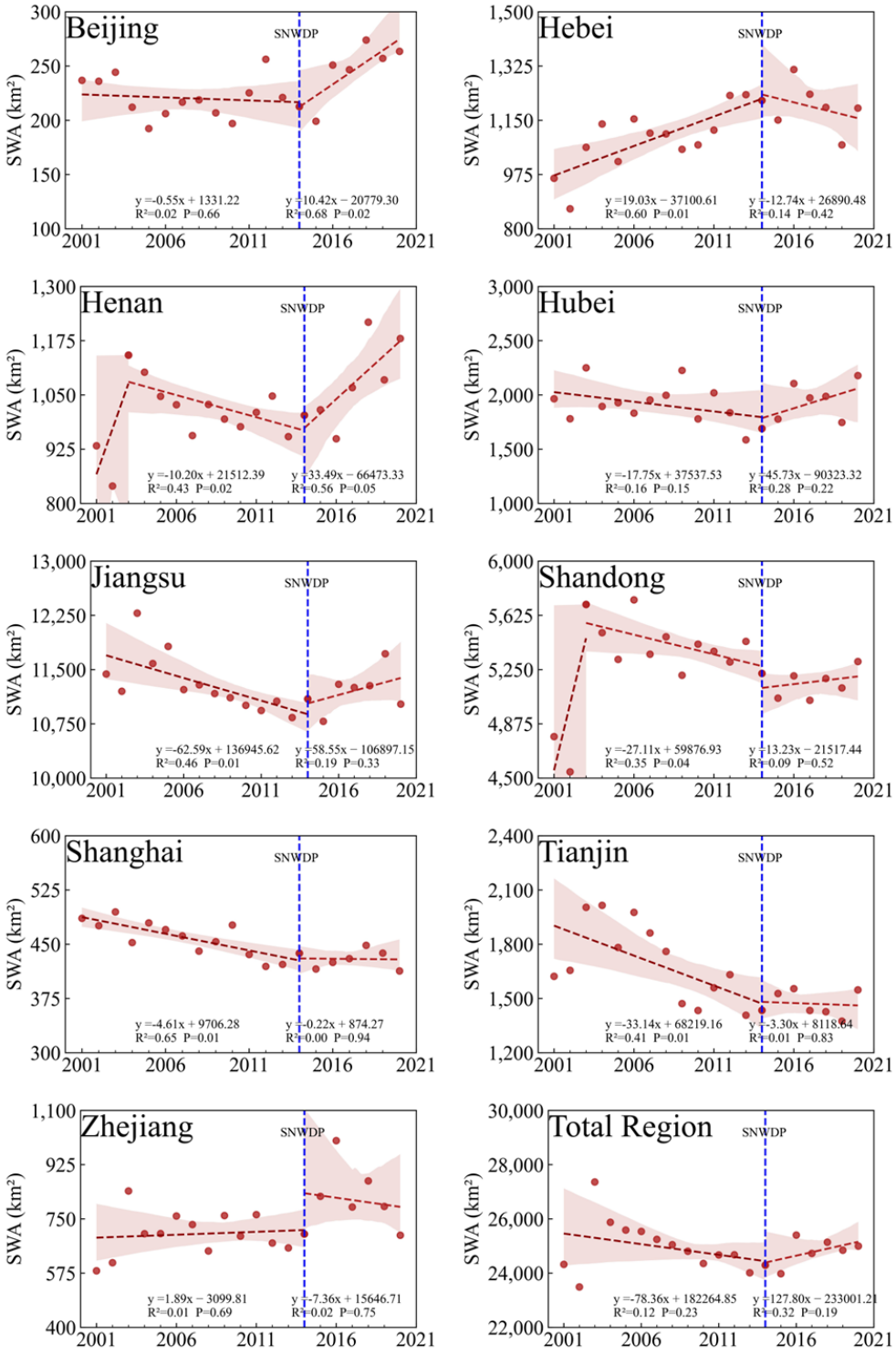

Figure 6. The trend regarding the max water bodies for different regions.

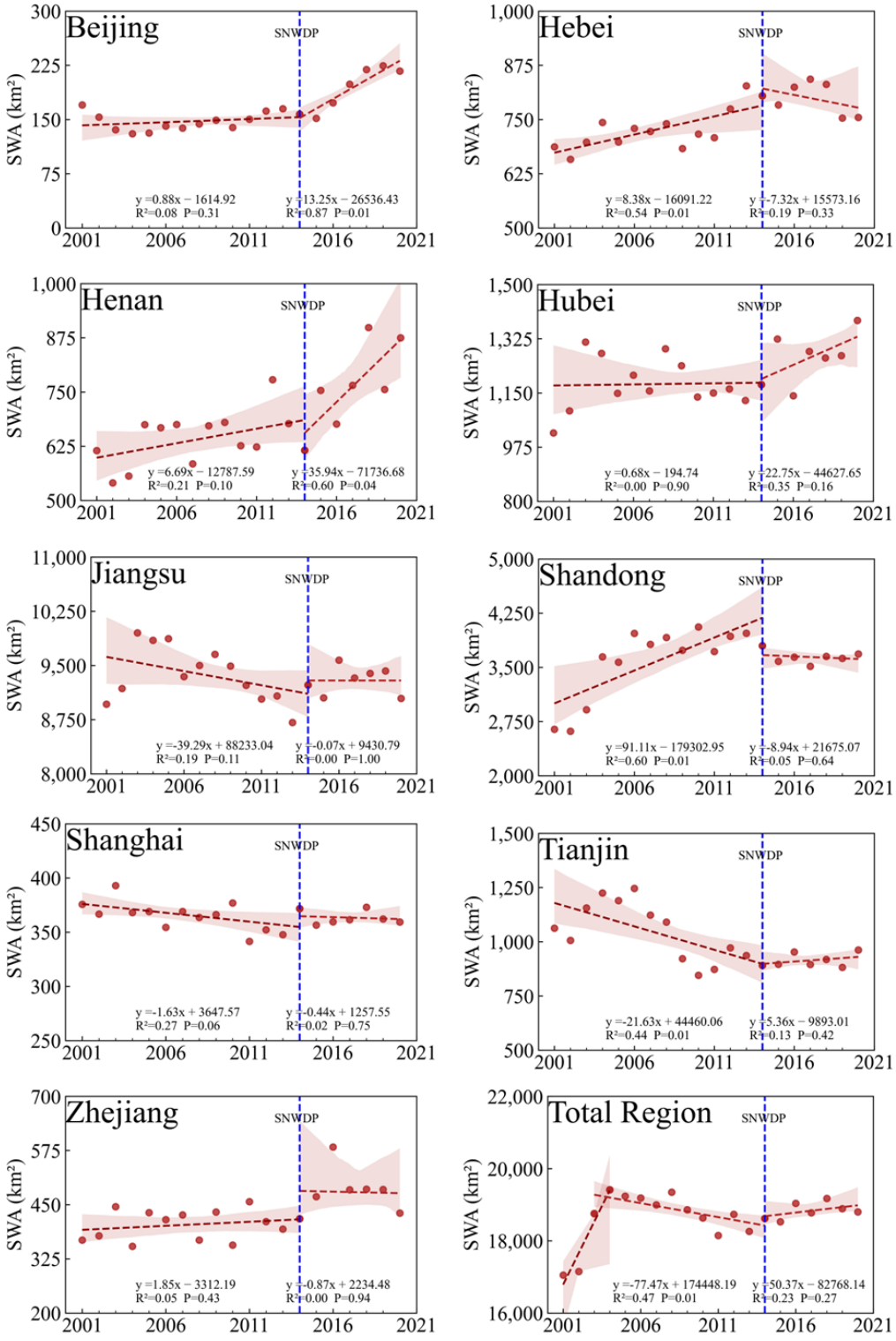

Figure 7. The change trend regarding the year-long water bodies in different regions.

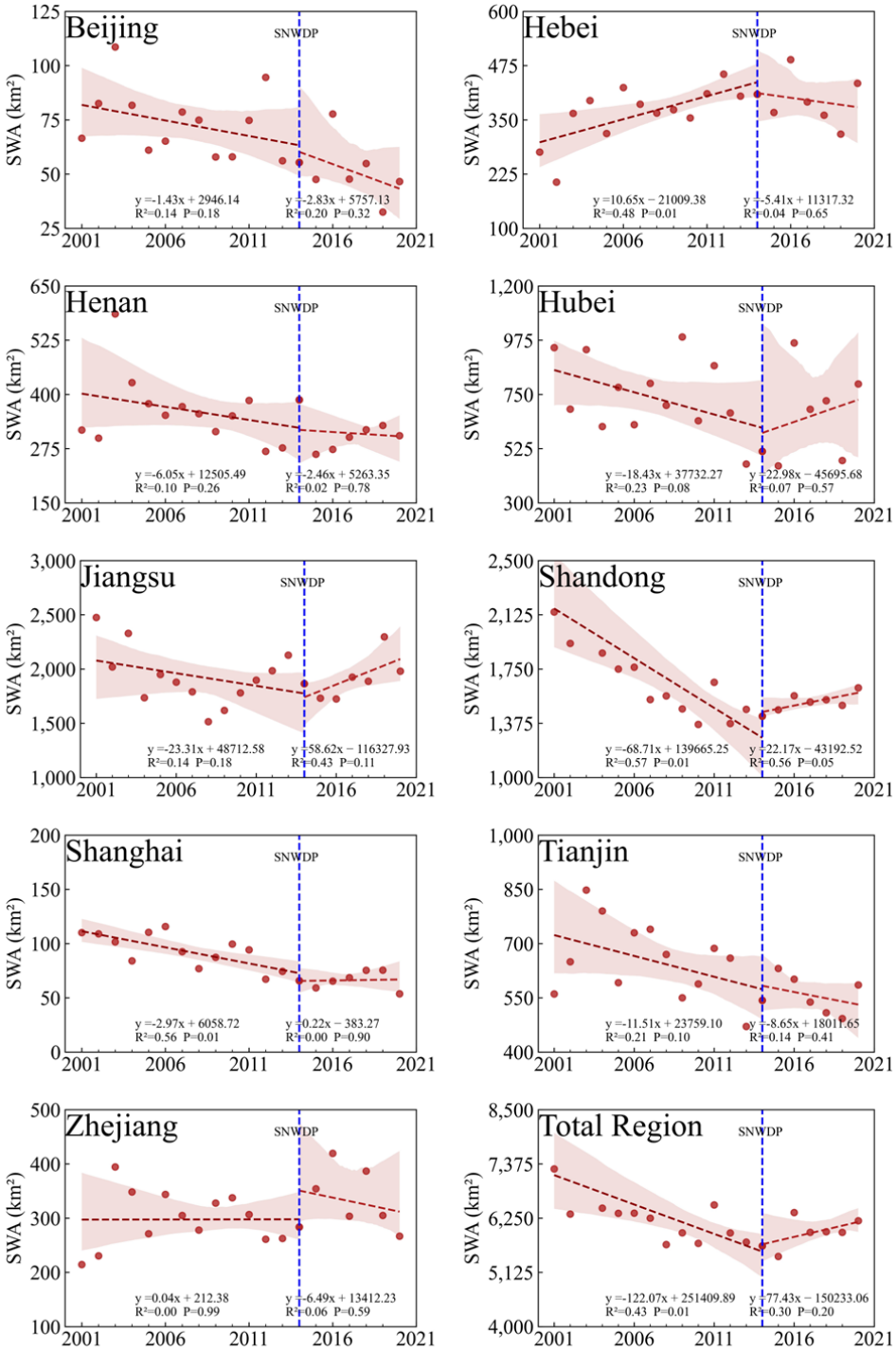

Figure 8. The change trend regarding the seasonal water bodies in different regions.

3.4. Detailed Spatial and Temporal Trends

The spatial and temporal trends regarding evapotranspiration (ET), temperature (Temp), and annual precipitation (AP) in the SNWDP-affected regions were analysed using the MK test, and our results are shown in Figure 9. The results revealed interesting findings. Regarding annual precipitation (AP), most areas within the zone of influence did not exhibit a significant trend, indicating a high level of AP volatility. However, certain areas in Shandong Province showed significant decreases in AP. Conversely, a few areas at the source of the eastern route displayed significant increases in AP.

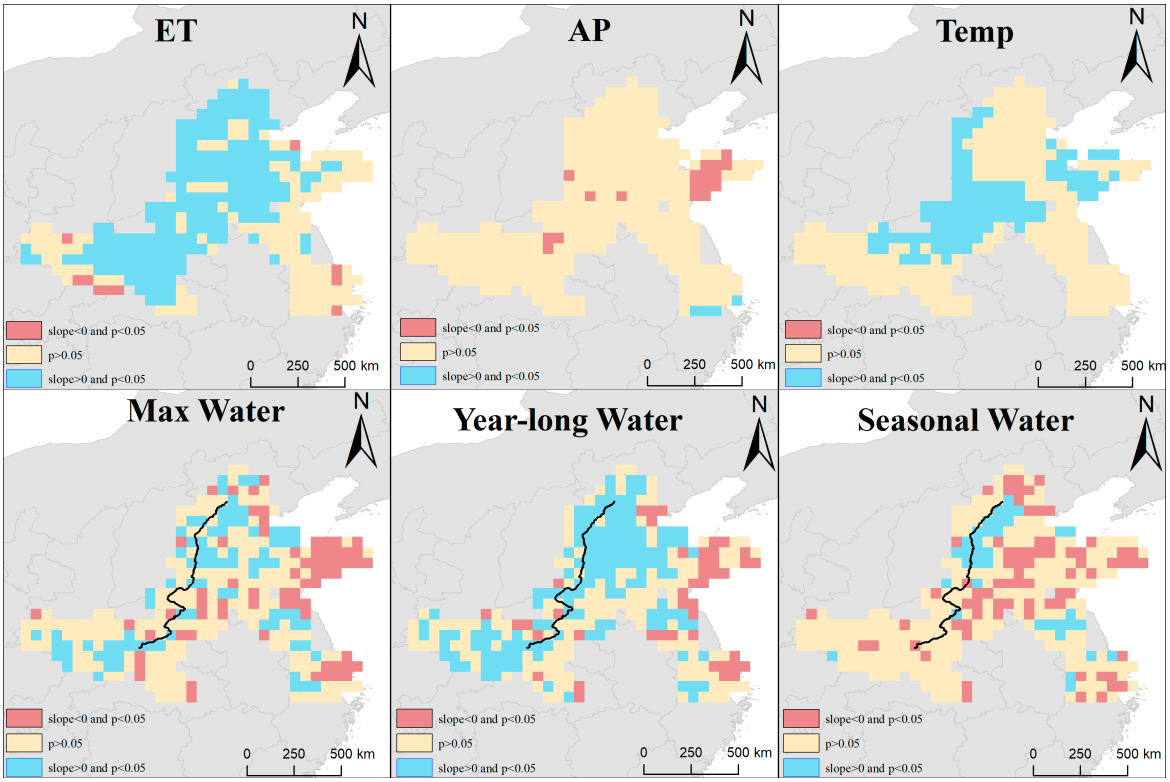

Figure 9. MK test results for 2001–2020 at a scale of 0.5° × 0.5°.

When analysing different water body types, significant increases in max water bodies in the southern source area of the central route and near the central route were observed. In the eastern route, the significant increases were mainly concentrated near Dongying City, Shandong Province. However, in Tianjin and most of the eastern part of Shandong Province, the max water body showed a significant decreasing trend. Year-long water body showed a significant increasing trend in most regions, except for Tianjin City. The regions around the central route all showed a significant increasing trend, revealing the effect of extra water supply in this area. The eastern Shandong Province and Shanghai City, which are distant from the route, continued to display a significantly decreasing trend in year-long water body.

In addition to the aforementioned trends, it is worth noting that the significant increases in seasonal water body were mainly concentrated in the Hebei Province section of the SNWDP's central route. This could potentially be attributed to China's ecological replenishment program, which has been in place since 2018. However, in the receiving areas located farther from the central route, there was predominantly a significant decrease in seasonal water body. The trend of seasonal water body in the eastern part of Shandong Province was the same as that of the max and year-long water bodies, which also showed a decreasing trend. However, it is important to note that Dongying city at the Yellow River estuary stood out as an exception, as it still showed a significant increasing trend in seasonal water body.

Based on this study, the trends of various components, including the max water body, year-long water body, seasonal water body, evapotranspiration (ET), annual precipitation (AP), and temperature (Temp), were analysed using the MK test. The analysis focused on the trends before and after the implementation of the SNWDP, using 2014 as the inflection point. The outcomes are presented in Figure 10. Upon dividing the data using 2014 as the breakpoint, it becomes evident that each component exhibits distinct trends before and after the implementation of the SNWDP. Our analysis allowed for a clear comparison between the pre-SNWDP and post-SNWDP periods, shedding light on the effects of this significant event on the studied components.

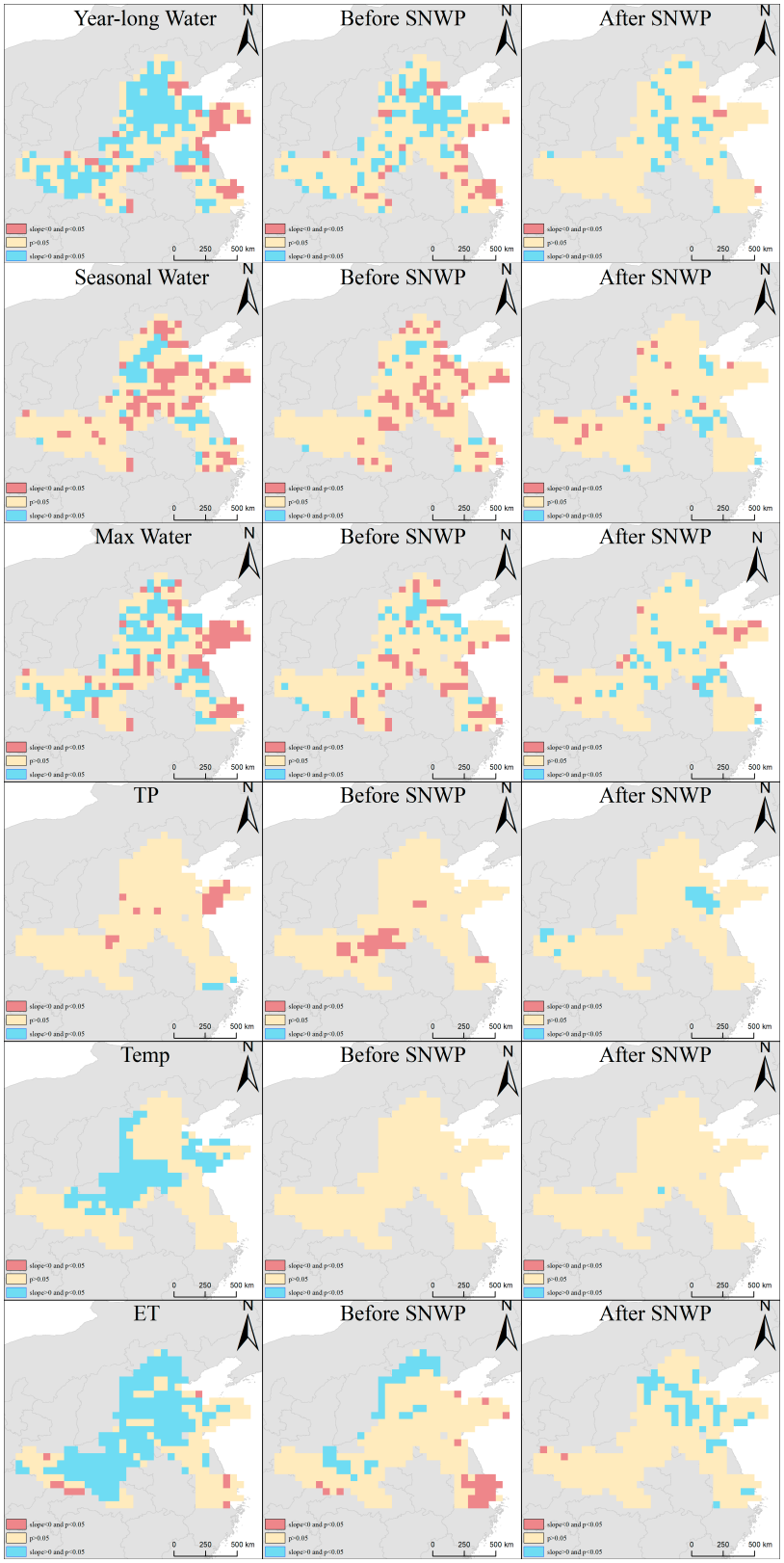

Figure 10. Trends before and after the implementation of the SNWDP at a scale of 0.5° × 0.5°.

The impact of the SNWDP event resulted in distinct changes in the year-long water body, max water body, and seasonal water body. Prior to the implementation of the SNWDP, there was a significant increase in year-long water body that was primarily concentrated near Shandong Province along the east route. Conversely, after the implementation

of the SNWDP, this prominent increase shifted towards the middle route. Furthermore, certain areas in the headwaters of the eastern route showed a notable decreasing trend prior to the implementation of the SNWDP, but this trend was no longer observed afterwards. It is worth mentioning that Tianjin continued to experience a decline even after the implementation of the SNWDP.

Following the implementation of the SNWDP, the regions where the max water body primarily increased were concentrated in the middle route area, the western part of Hebei Province, and Shandong Province. However, before the SNWDP, the increases were mainly concentrated in Shandong Province and the northern part of Hebei Province. With respect to seasonal water body, it is evident that before the SNWDP, only a few areas showed an upward trend, while many areas demonstrated a downward trend. However, after the SNWDP, the areas with significant decreases noticeably diminished, while the areas with significant increases expanded mainly along the central route, the northwestern part of Shandong Province, and the northern part of Jiangsu Province along the eastern route.

Prior to the SNWDP, Henan Province was the main region experiencing a significant decrease in annual precipitation (AP). However, after the implementation of the SNWDP, a significant increasing trend in AP was observed in northwestern Shandong Province. Although there was a noticeable upward trend in temperature between 2000 and 2020, this pattern did not continue after the division caused by the SNWDP. ET also exhibited varying patterns before and after the SNWDP, but generally maintained an increasing trend.

The surface water body in the study region primarily consists of rivers, lakes, and reservoirs, making it challenging to identify trends at a coarse scale of 0.5° × 0.5°. Therefore, in this study, we reanalysed the trends regarding seasonal and year-long water body before and after the implementation of the SNWDP using a finer 1 km × 1 km raster and the MK test. Figure 11 illustrates the changes in year-long and seasonal water body at the 1 km scale in various regions. It can be observed that the trend of river water body near the SNWDP area in Hebei Province can be clearly discerned.

The implementation of the SNWDP has had a positive impact on both seasonal and year-long water body. It reversed the declining trend witnessed by some rivers prior to 2014, leading to a clear upward trend in the downstream area near the central route. Specifically, the Miyun Reservoir, which is in the north end of the receiving area of the central route, experienced a significant increase in year-long water body after the implementation of the SNWDP. This increase has effectively alleviated the pressure on Beijing's water supply and contributed to the growth of the reservoir's water volume. Similarly, the Danjiangkou Reservoir, the source of the central route, has also seen a comparable and significant increase in surface water area after the implementation of the SNWDP.

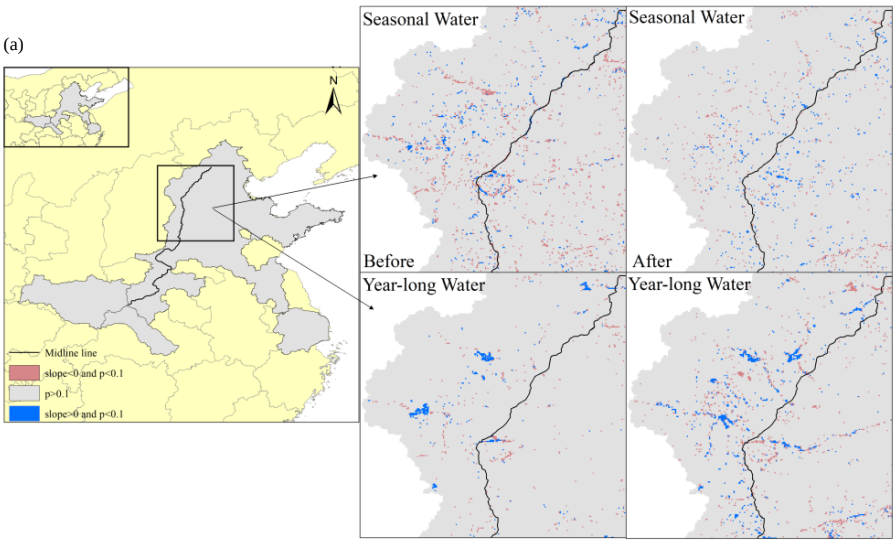

Figure 11. *Cont.*

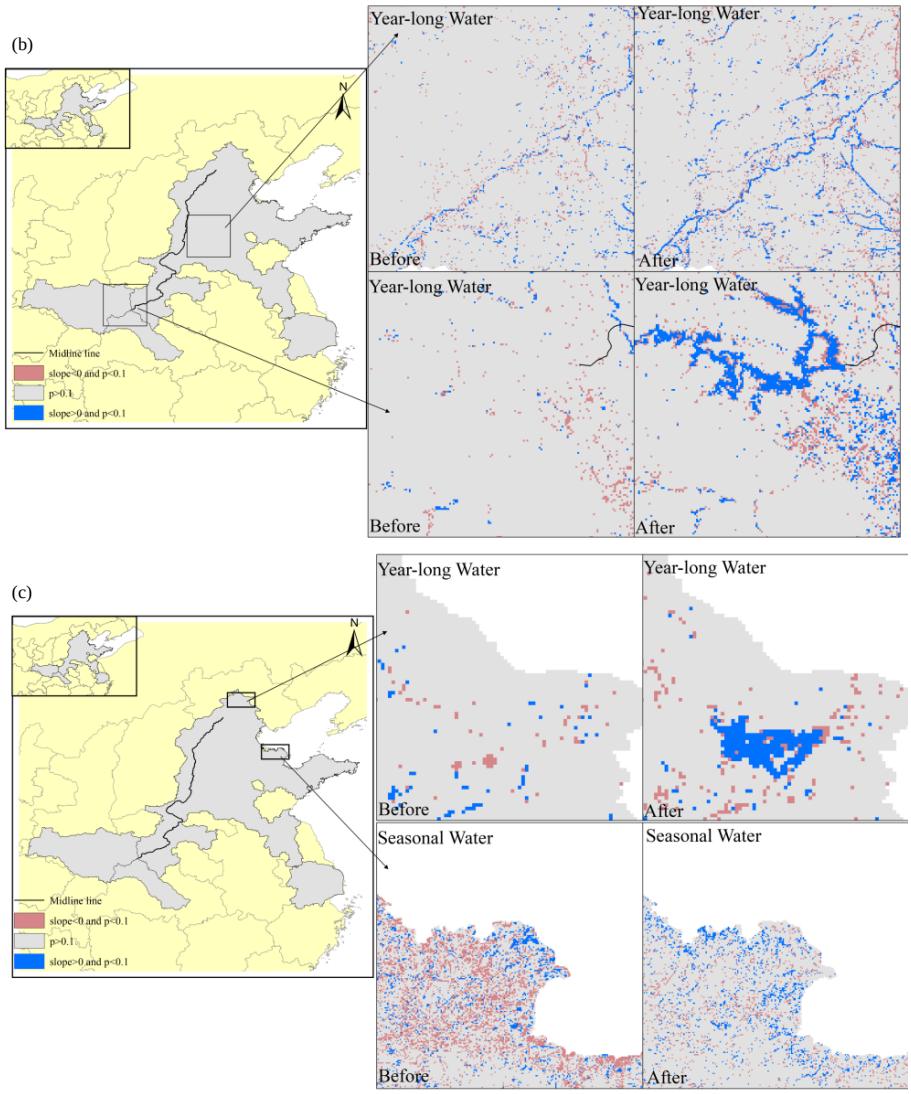

Figure 11. Trends before and after the implementation of the SNWDP at a scale of 1 km × 1 km in typical regions: (**a**) the part of the middle line project's zone of influence; (**b**) part of the central project's zone of influence and Danjiangkou reservoir; (**c**) Miyun reservoir and the part of the east line project's zone of influence.

3.5. Drivers of Change in Water Bodies

In this study, linear regression was employed as a tool to elucidate the factors influencing the alterations in the spatial extent of various water bodies within the recipient regions, as delineated in Table 2. Table 2 reveals that agricultural water consumption (Agcwu), AP, Temp, and SNWDP water transfer volume were the primary catalysts augmenting the area's year-long water, max water, and seasonal water bodies ($p < 0.01$ or $p < 0.05$). Conversely, industrial water consumption (Idswu) emerged as the principal factor contributing to the contraction of all the water bodies ($p < 0.01$).

In contrast, the study identified Cnspwu as a significant factor contributing to the decline in seasonal water. However, its impact on year-long water and max water was found to be statistically insignificant ($p > 0.1$). Furthermore, the influence of temperature on seasonal water was less pronounced ($p < 0.05$) compared to year-long water ($p < 0.01$) and max water ($p < 0.01$). These findings suggest that seasonal water is less susceptible to temperature fluctuations compared to its year-long and max counterparts.

Table 2. Factors influencing surface water areas, with SNWDP water transfer volume as the predictive variable.

	Year-Long	*p* Value	Max	*p* Value	Seasonal	*p* Value
Agcwu	1.07 ***	0.01	1.11 ***	0.01	1.21 ***	0.01
Idswu	−1.19 ***	0.01	−1.14 ***	0.01	−1.07 ***	0.01
Cnspwu	−0.02	0.94	−0.17	0.46	−0.52 **	0.02
ET	−1.92 ***	0.01	−1.97 ***	0.01	−2.03 ***	0.01
AP	1.14 ***	0.01	1.32 ***	0.01	1.63 ***	0.01
Temp	2.21 ***	0.01	2.04 ***	0.01	1.67 **	0.02
SNWDP	0.22 ***	0.01	0.21 ***	0.01	0.20 ***	0.01
Cons	3.57	0.43	3.79	0.40	2.42	0.40
R^2	0.65		0.67		0.71	

*** represents $p < 0.01$; ** represents $p < 0.05$; Cons is a constant term.

The regression results, presented in Tables 3 and 4, demonstrate that after replacing the water transfer volume variables with RWI or RSWI, the coefficients of RWI or RSWI all exhibited significant positive values. This reaffirms the positive impact of the SNWDP on the water bodies in the receiving area. It is important to note that the other variables did not undergo any significant changes. The results presented in Tables 3 and 4 can also be used as a robustness test, further validating the conclusions drawn in the previous regression analyses.

Table 3. Factors influencing surface water areas, with RWI as the predictive variable.

Factors	Year-Long	*p* Value	Max	*p* Value	Seasonal	*p* Value
Agcwu	1.05 ***	0.01	1.09 ***	0.01	1.19 ***	0.01
Idswu	−1.14 ***	0.01	−1.10 ***	0.01	−1.03 ***	0.01
Cnspwu	−0.86	0.94	−0.23	0.28	−0.58 ***	0.01
ET	−2.05 ***	0.01	−2.11 ***	0.01	−2.18 ***	0.01
AP	1.29 ***	0.01	1.47 ***	0.01	1.77 ***	0.01
Temp	1.84 ***	0.01	1.68 **	0.02	1.31 *	0.06
RWI	0.22 ***	0.01	0.08 ***	0.01	0.07 ***	0.01
Cons	4.43	0.28	4.65	0.25	3.31	0.40
R^2	0.69		0.71		0.75	

*** represents $p < 0.01$; ** represents $p < 0.05$; * represents $p < 0.1$; Cons is a constant term.

Table 4. Factors influencing surface water areas, with RSWI as the predictive variable.

Factors	Year-Long	*p* Value	Max	*p* Value	Seasonal	*p* Value
Agcwu	1.12 ***	0.01	1.15 ***	0.01	1.25 ***	0.01
Idswu	−1.31 ***	0.01	−1.26 ***	0.01	−1.18 ***	0.01
Cnspwu	−0.13	0.94	−0.28	0.24	−0.62	0.94
ET	−1.13 **	0.05	−1.19 **	0.03	−1.31 **	0.02
AP	1.16 ***	0.01	1.34 ***	0.01	1.67 ***	0.01
Temp	2.59 ***	0.01	2.41 ***	0.01	2.00 ***	0.01
RSWI	0.04 ***	0.01	0.04 ***	0.01	0.04 ***	0.01
Cons	−1.65	0.53	−1.34	0.74	−2.73	0.53
R^2	0.65		0.68		0.72	

*** represents $p < 0.01$; ** represents $p < 0.05$; Cons is a constant term.

In conclusion, the expansion of surface water body areas within the recipient regions was indeed positively influenced by the SNWDP, as well as the synergistic effects of regional water use structure and climatic conditions.

To further investigate the dynamics of water body transformations, we utilized the China Land Cover Dataset (CLCD) to explore the from–to transitions of water bodies in the replenishment regions. The results of the transition matrix are presented in Table 5. The primary transitions were from water to cropland and impervious surfaces, accounting for

areas of 720.53 km^2 and 400.87 km^2, respectively. The land types primarily transitioning into water were cropland, impervious surfaces, and barren land, with respective areas of 891.41 km^2, 311.27 km^2, and 303.16 km^2.

Table 5. Land use transfer matrix for 2013–2020 (km^2).

2013 \ 2020	Cropland	Forest	Shrub	Grassland	Water	Barren	Impervious
Cropland	211,081.60	1417.05	0.68	704.77	891.41	3.21	6527.16
Forest	1169.80	35,843.50	128.58	15.19	0.43	0	35.32
Shrub	1.38	68.81	332.84	93.38	0	0.014	0.014
Grassland	1339.15	843.26	65.77	8363.36	13.19	6.43	94.60
Water	720.53	3.53	0	1.70	5180.25	42.49	400.87
Barren	43.16	0.01	0	2.42	303.16	246.06	338.57
Impervious	13.16	0.01	0	0.16	311.27	2.21	62070.60

In aggregate, water area transitioned out with 1169.12 km^2, and other land use types transitioned into water with an area of 1519.46 km^2, resulting in a net increase of 350.34 km^2. Notably, cropland and impervious surfaces were the primary contributors to both water area outflow and inflow, while barren land emerged as a significant contributor to the inflow of water area. This suggests that the implementation of the SNWDP has facilitated ecological restoration by transforming barren land into water bodies.

Overall, our analysis of water body transitions using the CLCD provides valuable insights into the changes in land use patterns and the positive ecological outcomes resulting from the implementation of the SNWDP. These findings contribute to our understanding of the complex dynamics between water resources, land use, and ecological restoration in the replenishment regions.

4. Discussion

4.1. Reasons for Spatially Varied Changes

The limited availability of data at the sub-provincial level poses challenges to ascertaining the primary factors influencing the various changing types of surface water bodies across different provinces or cities through linear regression analysis. To address this limitation, correlation analysis was employed to investigate the influential factors impacting the changes in water bodies within each province or city, as depicted in Figure 12.

Figure 12 reveals the distinct factors influencing the water body changes in the different regions. In the central route areas, Beijing City, Hebei Province, and Henan Province show a high degree of similarity between their max water body and year-long water body. The South-to-North Water Diversion Project (SNWDP) has had a significant positive impact on the year-long water bodies in these three regions. As key replenishment areas for the central route, these regions benefit from regular water transfers and ecological replenishments during the flood season each year. These measures not only aid in the recovery of groundwater levels [65,66] but also positively influence surface water and ecological restoration [67]. The figure also illustrates the transformation among different water body types within these regions. Notably, Beijing City and Henan Province exhibit a significant negative correlation between their year-long water bodies and seasonal water bodies, indicating a clear trend of seasonal water bodies transitioning into year-long water bodies. The AP and Temp in the three regions show no significant correlation with water body area. These three changes in water body area in these regions are minimally affected by surface temperature and rainfall. ET and the perennial water bodies in the three regions exhibit a significant positive correlation, indicating that an increase in the surface water body area will further increase evaporation. This phenomenon may exacerbate water resource losses [68,69].

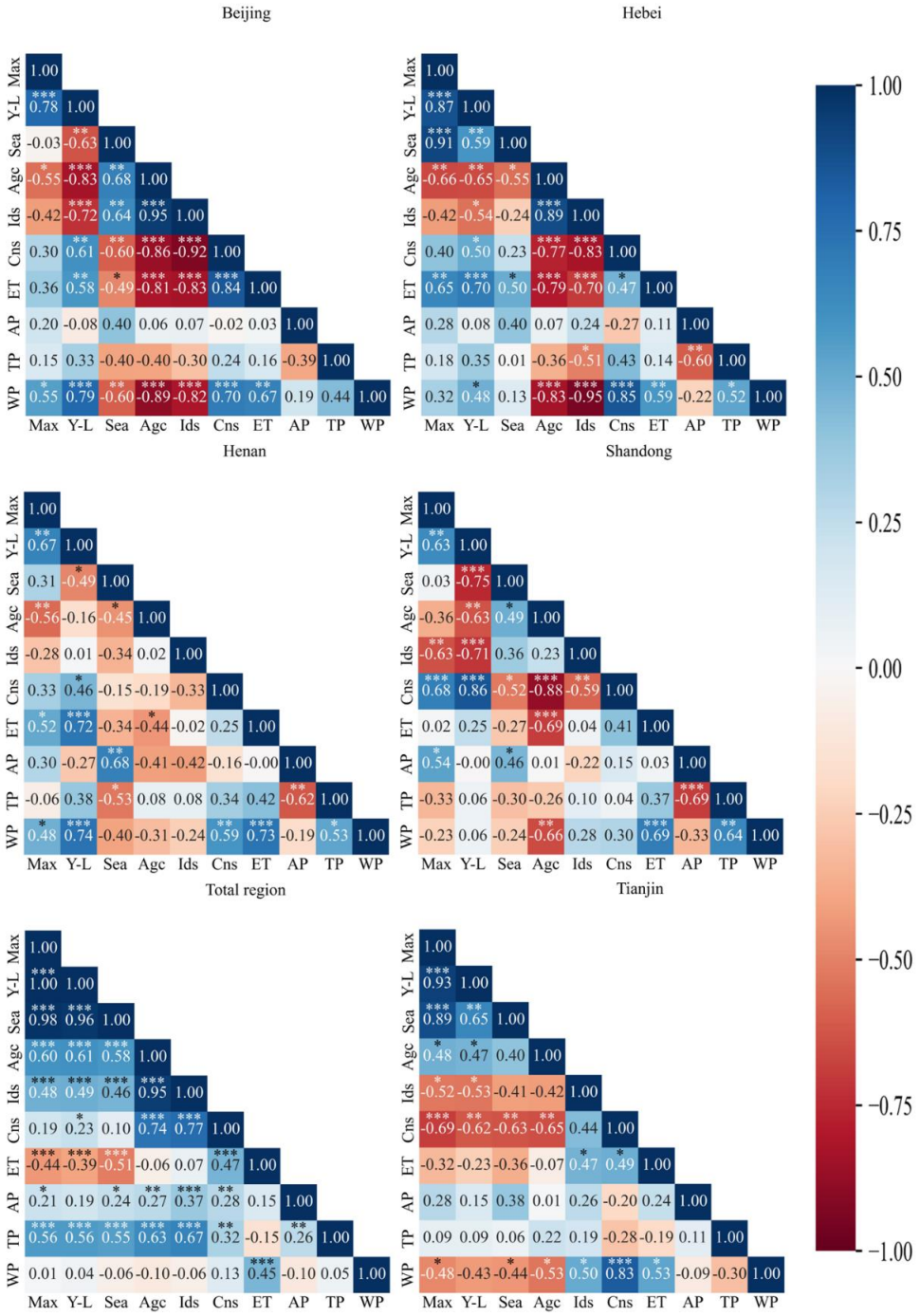

Figure 12. Graph showing correlation coefficients between water body areas and related factors. Max refers to max water body; Y-L refers to year-long water body; Sea refers to seasonal water body; Agc refers to agricultural water consumption (Agcwu); Ids refers to industrial water consumption (Idswu); Cns refers to the consumption of non-service public water use (Cnspwu); TP refers to 2 m height air temperature (Temp); WP refers to the water transfer volume of the SNWDP; ET refers to evapotranspiration; AP refers to annual precipitation. *** represents $p < 0.01$; ** represents $p < 0.05$; * represents $p < 0.1$.

Similarly, from Figure 12, we can see that Agcwu and Idswu are significantly negatively correlated with the year-long water body in three regions. Henan Province and Hebei Province, as important agricultural provinces in the North China Plain [70], consume a large amount of water resources annually for agricultural irrigation and agro-product processing, leading to the further depletion of water resources [71,72]. Moreover, Idswu and year-long

water body in Beijing City and Hebei Province show a significant positive correlation, while in Henan Province, there is no correlation. As a major agricultural rather than industrial province [73], Henan's industrial water consumption might have less impact on surface water compared to agricultural water use. However, as an important industrial base in North China, Hebei Province's industries require a large amount of water annually [74], which could lead to the depletion of groundwater and even a reduction in surface water area [75]. Therefore, it is crucial to reasonably adjust the water use structure in these three regions for the protection of surface water and water resources.

For Shandong Province, as seen in Figure 12, the three types of water bodies did not benefit from the SNWDP. Unlike the middle route project, the east route project does not involve extensive targeted ecological replenishment. Additionally, due to climate change and human activities, the region has been suffering from severe water shortages [76,77]. As an important base for aquaculture and land reclamation from the sea, the increase in surface water area in Shandong Province is likely due to the development of the aquaculture industry and the restoration of coastal lands [48,78,79] rather than being significantly related to the SNWDP. Similarly, the three types of water bodies in Tianjin City also did not benefit from the SNWDP, as the area also experienced substantial water losses. In terms of groundwater, the SNWDP has alleviated the losses in the region [80] but has not reversed the trend of continuous losses. Combining this with the trend graphs in Section 3.3 of our study, we believe that the SNWDP also mitigated the original surface water losses but did not significantly reverse this phenomenon. Furthermore, in Tianjin City, the year-long water body and seasonal water body show a significant positive correlation, indicating that under severe water loss, the surface water bodies in the region do not undergo mutual conversion but exhibit similar changing trends.

Moreover, it is important to note that the divergent changes in water bodies across different regions are not solely influenced by water transfers. Local water deficit levels, which vary from region to region, play a significant role. Areas with higher water deficits may experience more pronounced changes in water bodies as efforts are made to address water scarcity. Furthermore, the natural terrain features, such as terrain slope and the presence of rivers, lakes, and mountains, can also influence the distribution of water bodies and changes in water bodies within a region. To fully understand and manage the changes in water bodies, it is crucial to consider these local factors along with the effects of water transfers. By taking into account the unique characteristics of each region, water resource management strategies can be tailored to optimize water allocation, mitigate water deficits, and promote sustainable water use practices.

In conclusion, the findings demonstrate that changes in surface water bodies within the receiving areas are influenced not only by the South–North Water Diversion Project (SNWDP) but also by the climate environment, as well as the water usage structure. Therefore, rational water resource allocation and appropriate water usage structures play a crucial role in the preservation and management of water bodies within the receiving areas. It is important to consider these factors in order to ensure sustainable water management and the long-term health of the aquatic ecosystems in the region.

4.2. Impact of Recharge Intensity on Surface Water Bodies

We utilized two metrics, namely RWI (recharge intensity) and RWSI (recharge intensity of surface water), to represent the recharge intensity of the receiving areas of the South–North Water Diversion Project (SNWDP). The specific results are presented in Table 6. This table provides a visual representation of the impact of the SNWDP on different water body types across the studied regions. Comparing the correlation analysis results of Section 4.1 with the results in Table 6, the findings are largely consistent with those presented in Figure 12, further supporting the conclusions drawn earlier. When comparing RWI and RSWI, it is evident that the significance of the correlation coefficients using RSWI is markedly superior to that of RWI. This may be due to the fact that RSWI is constructed

from the max water body, enabling a more sensitive representation of the replenishment intensity of the SNWDP areas.

Table 6. Correlation coefficients between water body area and water diversion strength for different regions.

Region	RWI			RSWI		
	Year-Long	Seasonal	Max	Year-Long	Seasonal	Max
Total Region	0.157	0.045	0.122	0.125	0.096	0.032
Beijing	0.795 ***	−0.575 ***	0.570 **	0.463 **	−0.603 ***	0.458 **
Hebei	0.305	0.087	0.210	0.577 ***	0.160	0.392 *
Henan	0.740 ***	−0.325	0.539 **	0.715 ***	−0.363	0.667 ***
Shandong	0.043	−0.217	−0.224	0.060	−0.265	−0.259
Tianjin	−0.402 **	−0.459 **	−0.402 *	−0.449 **	−0.430 ***	−0.488 **

*** represents $p < 0.01$; ** represents $p < 0.05$; * represents $p < 0.1$.

4.3. Limitations and Perspectives

This study focuses on investigating the impact of the South-to-North Water Diversion Project (SNWDP) on surface water within the receiving area by analysing changes in the surface water area. Through rigorous temporal trend analysis and correlation analysis, this study provides valuable insights into the eco-hydrological effects of the SNWDP. However, it is important to acknowledge certain limitations that should be considered:

(1) Water body identification. Despite efforts to improve the water body extraction algorithm and minimize errors during water identification through remote sensing, there may still be inaccuracies that could lead to misclassified or omitted water bodies. These limitations could have potentially affected the accuracy of water body identification in this study.

(2) Complexity of surface water transformation. The transformation of surface water bodies is a complex phenomenon influenced by multiple factors. This study focused primarily on the connection between the SNWDP, meteorological factors, and water use factors that affect surface water area changes. However, to gain a more comprehensive understanding, future studies should explore the influence of other factors such as urbanization, water extraction, and the presence of artificial constructions that may also impact the mechanisms governing water body changes.

(3) Local topography and morphology. The sensitivity of surface water area alterations is also influenced by local topography and the morphology of rivers, lakes, and reservoirs. These factors were not fully accounted for in this study. To better elucidate the overall impact of the SNWDP on surface water bodies, future studies should consider these local variations. Incorporating topographic and morphological data will provide a more accurate assessment of the project's influence on surface water dynamics.

(4) The regions affected by the South-to-North Water Diversion Project (SNWDP) include a large number of rivers, lakes, and reservoirs. The relationship between the surface water area and the total water volume of these water bodies may not be a simple correlation. Therefore, when assessing changes in surface water area, this study could not accurately assess the changes in total water volume and water resources in these areas. This factor should be considered in future research.

5. Conclusions

This study investigated the impacts of the South-to-North Water Diversion Project (SNWDP) on surface water bodies from 2001 to 2020 based on long-term satellite observations. Our analysis focused on changes in water body areas before and after the SNWDP's implementation, as well as correlations with other relevant factors. The key findings are as follows:

(1) The impact of the SNWDP on the change in surface water area is heterogeneous, producing varying effects on different water bodies in different regions. Overall, the SNWDP has facilitated an increase in the year-long water body and max water body in the middle route area, while it has had almost no significant effect in the eastern route area. From a fine-scale perspective, the areas with a significant increase in surface water area are mainly concentrated near the middle route water transfer project and in Dongying City, Shandong Province. Both the Miyun Reservoir and the Danjiangkou Reservoir also show a significant increasing trend.

(2) The SNWDP played a significant role in the expansion of year-long water bodies, max water bodies, and seasonal water bodies within the total receiving areas. However, the impact of the SNWDP on surface water area varies in different regions, highlighting the importance of adjusting water usage structures accordingly to protect surface water. Barren is an important source transferring to water areas, and a pattern of seasonal water bodies transitioning into year-long water bodies has been observed in Beijing City and Henan Province, indicating that the implementation of the SNWDP has also contributed to the hydro ecological restoration of the receiving areas.

These findings highlight the diverse and specific effects of the SNWDP on different regions and water body types. These findings provide valuable insights for evaluating the environmental and global changes resulting from significant human interventions. Additionally, they are particularly beneficial for policymakers and decision makers engaged in managing water resources. The diverse impacts of the SNWDP on different regions and water body types emphasize the need for tailored strategies in water management and resource allocation.

Author Contributions: Conceptualization, T.G. and R.L.; methodology, T.G.; software, T.G.; validation, P.C., H.F. and X.S.; formal analysis, T.G.; investigation, J.G.; resources, T.G.; data curation, T.G.; writing—original draft preparation, T.G.; writing—review and editing, X.Z.; visualization, Z.X.; supervision, R.L.; project administration, R.L.; funding acquisition, R.L. All authors have read and agreed to the published version of the manuscript.

Funding: This research was funded by the National Key Research and Development Program of China (Grant No. 2020YFC1807103), the National Natural Science Foundation of China (Grant No. 42341206), Network Security and Informatization Special Application Demonstration Project of Chinese Academy of Sciences (CAS-WX2023SF-040301), and the Fundamental Research Funds for the Central Universities (E3E40503X2).

Data Availability Statement: The ERA5-land data, ET data, Dem data, and remote sensing data are all available at https://developers.google.com/earth-engine/datasets/ (accessed on 1 October 2022). Statistical data are available in the provincial water statistics bulletins. The land cover data are available at https://zenodo.org/record/5816591 (accessed on 1 October 2022). The fundamental geographic element data are available at http://www.ngcc.cn/ngcc/ (accessed on 1 October 2022).

Acknowledgments: We thank the reviewers for their valuable comments.

Conflicts of Interest: The authors declare that they have no conflicts of interests.

References

1. Shen, Z.; Zhang, Q.; Singh, V.P.; Pokhrel, Y.; Li, J.; Xu, C.-Y.; Wu, W. Drying in the Low-Latitude Atlantic Ocean Contributed to Terrestrial Water Storage Depletion across Eurasia. *Nat. Commun.* **2022**, *13*, 1849. [CrossRef] [PubMed]
2. Wang, X.; Xiao, X.; Zou, Z.; Dong, J.; Qin, Y.; Doughty, R.B.; Menarguez, M.A.; Chen, B.; Wang, J.; Ye, H.; et al. Gainers and Losers of Surface and Terrestrial Water Resources in China during 1989–2016. *Nat. Commun.* **2020**, *11*, 3471. [CrossRef]
3. Ma, T.; Sun, S.; Fu, G.; Hall, J.W.; Ni, Y.; He, L.; Yi, J.; Zhao, N.; Du, Y.; Pei, T.; et al. Pollution Exacerbates China's Water Scarcity and Its Regional Inequality. *Nat. Commun.* **2020**, *11*, 650. [CrossRef] [PubMed]
4. Piao, S.; Ciais, P.; Huang, Y.; Shen, Z.; Peng, S.; Li, J.; Zhou, L.; Liu, H.; Ma, Y.; Ding, Y.; et al. The Impacts of Climate Change on Water Resources and Agriculture in China. *Nature* **2010**, *467*, 43–51. [CrossRef] [PubMed]
5. Wang, J.; Li, Y.; Huang, J.; Yan, T.; Sun, T. Growing Water Scarcity, Food Security and Government Responses in China. *Glob. Food Secur.* **2017**, *14*, 9–17. [CrossRef]
6. Li, P.; Qian, H. Water Resources Research to Support a Sustainable China. *Int. J. Water Resour. Dev.* **2018**, *34*, 327–336. [CrossRef]

7. Zhao, S.; Liu, W.; Zhu, M.; Ma, Y.; Li, Z. A Priority-Based Multi-Objective Framework for Water Resources Diversion and Allocation in the Middle Route of the South-to-North Water Diversion Project. *Socio-Econ. Plan. Sci.* **2021**, *78*, 101085. [CrossRef]
8. He, Y.; Wang, Y.; Chen, X. Spatial Patterns and Regional Differences of Inequality in Water Resources Exploitation in China. *J. Clean. Prod.* **2019**, *227*, 835–848. [CrossRef]
9. Zhao, F.; Wang, X.; Wu, Y.; Singh, S.K. Prefectures Vulnerable to Water Scarcity Are Not Evenly Distributed across China. *Commun. Earth Environ.* **2023**, *4*, 145. [CrossRef]
10. Varis, O.; Vakkilainen, P. China's 8 Challenges to Water Resources Management in the First Quarter of the 21st Century. *Geomorphology* **2001**, *41*, 93–104. [CrossRef]
11. Liu, M.; Wei, J.; Wang, G.; Wang, F. Water Resources Stress Assessment and Risk Early Warning—A Case of Hebei Province China. *Ecol. Indic.* **2017**, *73*, 358–368. [CrossRef]
12. Zuo, L.; Zhang, Z.; Carlson, K.M.; MacDonald, G.K.; Brauman, K.A.; Liu, Y.; Zhang, W.; Zhang, H.; Wu, W.; Zhao, X.; et al. Progress towards Sustainable Intensification in China Challenged by Land-Use Change. *Nat. Sustain.* **2018**, *1*, 304–313. [CrossRef]
13. Qin, J.; Ding, Y.-J.; Zhao, Q.-D.; Wang, S.-P.; Chang, Y.-P. Assessments on Surface Water Resources and Their Vulnerability and Adaptability in China. *Adv. Clim. Chang. Res.* **2020**, *11*, 381–391. [CrossRef]
14. He, C.; He, X.; Fu, L. China's South-to-North Water Transfer Project: Is It Needed? China's South-to-North Water Transfer Project. *Geogr. Compass* **2010**, *4*, 1312–1323. [CrossRef]
15. Kattel, G.R.; Shang, W.; Wang, Z.; Langford, J. China's South-to-North Water Diversion Project Empowers Sustainable Water Resources System in the North. *Sustainability* **2019**, *11*, 3735. [CrossRef]
16. Peng, Z.; Yin, J.; Zhang, L.; Zhao, J.; Liang, Y.; Wang, H. Assessment of the Socio-Economic Impactof a Water Diversion Project Fora Water-Receiving Area. *Pol. J. Environ. Stud.* **2020**, *29*, 1771–1784. [CrossRef]
17. Long, Y.; Li, Y.; Lei, X.; Hou, Y.; Guo, S.; Sun, J. A Study on Comprehensive Evaluation Methods for Coordinated Development of Water Diversion Projects Based on Advanced SWOT Analysis and Coupling Coordination Model. *Sustainability* **2021**, *13*, 13600. [CrossRef]
18. Gao, W.; Zeng, Y.; Liu, Y.; Wu, B. Human Activity Intensity Assessment by Remote Sensing in the Water Source Area of the Middle Route of the South-to-North Water Diversion Project in China. *Sustainability* **2019**, *11*, 5670. [CrossRef]
19. Zhang, J.; Zhang, Y.; Sun, G.; Song, C.; Dannenberg, M.P.; Li, J.; Liu, N.; Zhang, K.; Zhang, Q.; Hao, L. Vegetation Greening Weakened the Capacity of Water Supply to China's South-to-North Water Diversion Project. Hydrol. *Earth Syst. Sci.* **2021**, *25*, 5623–5640. [CrossRef]
20. Yang, Z.; Huang, X.; Fang, G.; Ye, J.; Lu, C. Benefit Evaluation of East Route Project of South to North Water Transfer Based on Trapezoid Cloud Model. *Agric. Water Manag.* **2021**, *254*, 106960. [CrossRef]
21. Tan, L.; Luo, W.; Yang, B.; Huang, M.; Shuai, S.; Cheng, C.; Zhou, X.; Li, M.; Hu, C. Evaluation of Landscape Ecological Risk in Key Ecological Functional Zone of South–to–North Water Diversion Project, China. *Ecol. Indic.* **2023**, *147*, 109934. [CrossRef]
22. Rogers, S.; Barnett, J.; Webber, M.; Finlayson, B.; Wang, M. Governmentality and the Conduct of Water: China's South–North Water Transfer Project. *Trans. Inst. Br. Geogr.* **2016**, *41*, 429–441. [CrossRef]
23. Wang, K.; Wang, Z.; Liu, K.; Cheng, L.; Wang, L.; Ye, A. Impacts of the Eastern Route of the South-to-North Water Diversion Project Emergency Operation on Flooding and Drainage in Water-Receiving Areas: An Empirical Case in China. *Nat. Hazards Earth Syst. Sci.* **2019**, *19*, 555–570. [CrossRef]
24. Long, D.; Yang, W.; Scanlon, B.R.; Zhao, J.; Liu, D.; Burek, P.; Pan, Y.; You, L.; Wada, Y. South-to-North Water Diversion Stabilizing Beijing's Groundwater Levels. *Nat. Commun.* **2020**, *11*, 3665. [CrossRef]
25. Zhang, C.; Duan, Q.; Yeh, P.J.F.; Pan, Y.; Gong, H.; Moradkhani, H.; Gong, W.; Lei, X.; Liao, W.; Xu, L.; et al. Sub-Regional Groundwater Storage Recovery in North China Plain after the South-to-North Water Diversion Project. *J. Hydrol.* **2021**, *597*, 126156. [CrossRef]
26. Du, Z.; Ge, L.; Ng, A.H.-M.; Lian, X.; Zhu, Q.; Horgan, F.G.; Zhang, Q. Analysis of the Impact of the South-to-North Water Diversion Project on Water Balance and Land Subsidence in Beijing, China between 2007 and 2020. *J. Hydrol.* **2021**, *603*, 126990. [CrossRef]
27. Abbott, B.W.; Bishop, K.; Zarnetske, J.P.; Minaudo, C.; Chapin, F.S.; Krause, S.; Hannah, D.M.; Conner, L.; Ellison, D.; Godsey, S.E.; et al. Human Domination of the Global Water Cycle Absent from Depictions and Perceptions. *Nat. Geosci.* **2019**, *12*, 533–540. [CrossRef]
28. Subin, Z.M.; Riley, W.J.; Mironov, D. An Improved Lake Model for Climate Simulations: Model Structure, Evaluation, and Sensitivity Analyses in CESM1. *J. Adv. Model. Earth Syst.* **2012**, *4*, M02001. [CrossRef]
29. Su, D.; Wen, L.; Huang, A.; Wu, Y.; Gao, X.; Wang, M.; Zhao, Y.; Kirillin, G. Simulation of the Potential Impacts of Lakes on Glacier Behavior over the Tibetan Plateau in Summer. *Clim. Dyn.* **2023**, *60*, 3435–3454. [CrossRef]
30. Woolway, R.I.; Huang, L.; Sharma, S.; Lee, S.; Rodgers, K.B.; Timmermann, A. Lake Ice Will Be Less Safe for Recreation and Transportation under Future Warming. *Earth's Future* **2022**, *10*, e2022EF002907. [CrossRef]
31. Erler, A.R.; Frey, S.K.; Khader, O.; d'Orgeville, M.; Park, Y.; Hwang, H.; Lapen, D.R.; Richard Peltier, W.; Sudicky, E.A. Simulating Climate Change Impacts on Surface Water Resources within a Lake-Affected Region Using Regional Climate Projections. *Water Resour. Res.* **2019**, *55*, 130–155. [CrossRef]
32. Tiwari, A.D.; Pokhrel, Y.; Kramer, D.; Akhter, T.; Tang, Q.; Liu, J.; Qi, J.; Loc, H.H.; Lakshmi, V. A Synthesis of Hydroclimatic, Ecological, and Socioeconomic Data for Transdisciplinary Research in the Mekong. *Sci. Data* **2023**, *10*, 283. [CrossRef] [PubMed]

33. Vörösmarty, C.J.; Green, P.; Salisbury, J.; Lammers, R.B. Global Water Resources: Vulnerability from Climate Change and Population Growth. *Sci. New Ser.* **2000**, *289*, 284–288. [CrossRef] [PubMed]
34. Ren, G.; Liu, H.; Chu, Z.; Zhang, L.; Li, X.; Li, W.; Chen, Y.; Gao, G.; Zhang, Y. Multi-Time-Scale Climatic Variations over Eastern China and Implications for the South–North Water Diversion Project. *J. Hydrometeorol.* **2011**, *12*, 600–617. [CrossRef]
35. Xu, Y.; Xu, X.; Tang, Q. Human Activity Intensity of Land Surface: Concept, Methods and Application in China. *J. Geogr. Sci.* **2016**, *26*, 1349–1361. [CrossRef]
36. Li, Z.; Liu, Y. Research on the Spatial Distribution Pattern and Influencing Factors of Digital Economy Development in China. *IEEE Access* **2021**, *9*, 63094–63106. [CrossRef]
37. Wang, J.; Han, Q.; Wu, K.; Xu, Z.; Liu, P. Spatial-Temporal Patterns and Evolution Characteristics of the Coordinated Development of Industrial Economy, Natural Resources and Environment in China. *Resour. Policy* **2022**, *75*, 102463. [CrossRef]
38. Zhao, A.; Xiang, K.; Zhang, A.; Zhang, X. Spatial-Temporal Evolution of Meteorological and Groundwater Droughts and Their Relationship in the North China Plain. *J. Hydrol.* **2022**, *610*, 127903. [CrossRef]
39. Li, Y.; Xiong, W.; Zhang, W.; Wang, C.; Wang, P. Life Cycle Assessment of Water Supply Alternatives in Water-Receiving Areas of the South-to-North Water Diversion Project in China. *Water Res.* **2016**, *89*, 9–19. [CrossRef]
40. Gao, W.; Zeng, Y.; Zhao, D.; Wu, B.; Ren, Z. Land Cover Changes and Drivers in the Water Source Area of the Middle Route of the South-to-North Water Diversion Project in China from 2000 to 2015. *Chin. Geogr. Sci.* **2020**, *30*, 115–126. [CrossRef]
41. Zhong, H.; Liao, T.; Fang, G.; Ren, K.; Zhang, S. Exploring Optimal Joint Operating Rules for Large-Scale Inter-Basin Water Transfer Projects with Multiple Water Sources, Diversion Routes, and Water Demand Areas. *J. Hydrol. Reg. Stud.* **2023**, *49*, 101504. [CrossRef]
42. Lv, A.; Han, Y.; Zhu, W.; Zhang, S.; Zhao, W. Risk Assessment of Water Resources Carrying Capacity in China. *J. Am. Water Resour. Assoc.* **2021**, *57*, 539–551. [CrossRef]
43. Han, Y.; Zhang, S.; Lv, A.; Zeng, H. Risk Assessment of the Water Resources Carrying Capacity: A Case Study in North China. *J. Am. Water Resour. Assoc.* **2022**, *58*, 1240–1254. [CrossRef]
44. Liu, J.; Li, M.; Wu, M.; Luan, X.; Wang, W.; Yu, Z. Influences of the South–to-North Water Diversion Project and Virtual Water Flows on Regional Water Resources Considering both Water Quantity and Quality. *J. Clean. Prod.* **2020**, *244*, 118920. [CrossRef]
45. Liu, Y.; Xin, Z.; Sun, S.; Zhang, C.; Fu, G. Assessing Environmental, Economic, and Social Impacts of Inter-Basin Water Transfer in China. *J. Hydrol.* **2023**, *625*, 130008. [CrossRef]
46. Li, Y.; Dang, B.; Zhang, Y.; Du, Z. Water Body Classification from High-Resolution Optical Remote Sensing Imagery: Achievements and Perspectives. *ISPRS J. Photogramm. Remote Sens.* **2022**, *187*, 306–327. [CrossRef]
47. Chen, J.; Chen, S.; Fu, R.; Li, D.; Jiang, H.; Wang, C.; Peng, Y.; Jia, K.; Hicks, B.J. Remote Sensing Big Data for Water Environment Monitoring: Current Status, Challenges, and Future Prospects. *Earth's Future* **2022**, *10*, e2021EF002289. [CrossRef]
48. Zhou, Y.; Dong, J.; Cui, Y.; Zhou, S.; Li, Z.; Wang, X.; Deng, X.; Zou, Z.; Xiao, X. Rapid Surface Water Expansion Due to Increasing Artificial Reservoirs and Aquaculture Ponds in North China Plain. *J. Hydrol.* **2022**, *608*, 127637. [CrossRef]
49. Zhou, Y.; Dong, J.; Cui, Y.; Zhao, M.; Wang, X.; Tang, Q.; Zhang, Y.; Zhou, S.; Metternicht, G.; Zou, Z.; et al. Ecological Restoration Exacerbates the Agriculture-Induced Water Crisis in North China Region. *Agric. For. Meteorol.* **2023**, *331*, 109341. [CrossRef]
50. Yang, X.; Qin, Q.; Grussenmeyer, P.; Koehl, M. Urban Surface Water Body Detection with Suppressed Built-up Noise Based on Water Indices from Sentinel-2 MSI Imagery. *Remote Sens. Environ.* **2018**, *219*, 259–270. [CrossRef]
51. Li, Z.; Zhang, X.; Xiao, P. Spectral Index-Driven FCN Model Training for Water Extraction from Multispectral Imagery. *ISPRS J. Photogramm. Remote Sens.* **2022**, *192*, 344–360. [CrossRef]
52. Zou, Z.; Xiao, X.; Dong, J.; Qin, Y.; Doughty, R.B.; Menarguez, M.A.; Zhang, G.; Wang, J. Divergent Trends of Open-Surface Water Body Area in the Contiguous United States from 1984 to 2016. *Proc. Natl. Acad. Sci. USA* **2018**, *115*, 3810–3815. [CrossRef]
53. Wang, X.; Xiao, X.; Qin, Y.; Dong, J.; Wu, J.; Li, B. Improved Maps of Surface Water Bodies, Large Dams, Reservoirs, and Lakes in China. *Earth Syst. Sci. Data* **2022**, *14*, 3757–3771. [CrossRef]
54. Muñoz-Sabater, J.; Dutra, E.; Agustí-Panareda, A.; Albergel, C.; Arduini, G.; Balsamo, G.; Boussetta, S.; Choulga, M.; Harrigan, S.; Hersbach, H.; et al. ERA5-Land: A State-of-the-Art Global Reanalysis Dataset for Land Applications. *Earth Syst. Sci. Data* **2021**, *13*, 4349–4383. [CrossRef]
55. Jiao, D.; Xu, N.; Yang, F.; Xu, K. Evaluation of Spatial-Temporal Variation Performance of ERA5 Precipitation Data in China. *Sci. Rep.* **2021**, *11*, 17956. [CrossRef] [PubMed]
56. Xu, J.; Ma, Z.; Yan, S.; Peng, J. Do ERA5 and ERA5-Land Precipitation Estimates Outperform Satellite-Based Precipitation Products? A Comprehensive Comparison between State-of-the-Art Model-Based and Satellite-Based Precipitation Products over Mainland China. *J. Hydrol.* **2022**, *605*, 127353. [CrossRef]
57. Running, S.; Mu, Q.; Zhao, M. MOD16A2 MODIS/Terra Net Evapotranspiration 8-Day L4 Global 500m SIN Grid V006 [Data Set]. 2017. Available online: https://lpdaac.usgs.gov/products/mod16a2v006/ (accessed on 6 October 2023).
58. Takaku, J.; Tadono, T.; Tsutsui, K.; Ichikawa, M. Validation of "AW3D" Global DSM Generated from ALOS PRISM. In Proceedings of the ISPRS Annals of the Photogrammetry, Remote Sensing and Spatial Information Sciences, Prague, Czech Republic, 12–19 July 2016; Volume III-4, pp. 25–31. [CrossRef]
59. Yang, J.; Huang, X. The 30 m Annual Land Cover Dataset and Its Dynamics in China from 1990 to 2019. *Earth Syst. Sci. Data* **2021**, *13*, 3907–3925. [CrossRef]

60. Zou, Z.; Dong, J.; Menarguez, M.A.; Xiao, X.; Qin, Y.; Doughty, R.B.; Hooker, K.V.; David Hambright, K. Continued Decrease of Open Surface Water Body Area in Oklahoma during 1984–2015. *Sci. Total Environ.* **2017**, *595*, 451–460. [CrossRef]
61. Gong, P.; Li, X.; Wang, J.; Bai, Y.; Chen, B.; Hu, T.; Liu, X.; Xu, B.; Yang, J.; Zhang, W.; et al. Annual Maps of Global Artificial Impervious Area (GAIA) between 1985 and 2018. *Remote Sens. Environ.* **2020**, *236*, 111510. [CrossRef]
62. Xia, H.; Zhao, J.; Qin, Y.; Yang, J.; Cui, Y.; Song, H.; Ma, L.; Jin, N.; Meng, Q. Changes in Water Surface Area during 1989–2017 in the Huai River Basin Using Landsat Data and Google Earth Engine. *Remote Sens.* **2019**, *11*, 1824. [CrossRef]
63. Mann, H.B. Nonparametric Tests Against Trend. *Econometrica* **1945**, *13*, 245. [CrossRef]
64. Sen, P.K. Estimates of the Regression Coefficient Based on Kendall's Tau. *J. Am. Stat. Assoc.* **1968**, *63*, 1379–1389. [CrossRef]
65. Zhang, C.; Duan, Q.; Yeh, P.J.-F.; Pan, Y.; Gong, H.; Gong, W.; Di, Z.; Lei, X.; Liao, W.; Huang, Z.; et al. The Effectiveness of the South-to-North Water Diversion Middle Route Project on Water Delivery and Groundwater Recovery in North China Plain. *Water Resour. Res.* **2020**, *56*, e2019WR026759. [CrossRef]
66. Liu, J.; Jiang, L.; Zhang, X.; Druce, D.; Kittel, C.M.M.; Tøttrup, C.; Bauer-Gottwein, P. Impacts of Water Resources Management on Land Water Storage in the North China Plain: Insights from Multi-Mission Earth Observations. *J. Hydrol.* **2021**, *603*, 126933. [CrossRef]
67. Liu, H.; Wu, J.; Liao, M. Ecosystem Service Trade-Offs Upstream and Downstream of a Dam: A Case Study of the Danjiangkou Dam, China. *Arab. J. Geosci.* **2019**, *12*, 17. [CrossRef]
68. Zhan, S.; Song, C.; Wang, J.; Sheng, Y.; Quan, J. A Global Assessment of Terrestrial Evapotranspiration Increase Due to Surface Water Area Change. *Earth's Future* **2019**, *7*, 266–282. [CrossRef]
69. Condon, L.E.; Atchley, A.L.; Maxwell, R.M. Evapotranspiration Depletes Groundwater under Warming over the Contiguous United States. *Nat. Commun.* **2020**, *11*, 873. [CrossRef] [PubMed]
70. Zhang, Y.; Qi, Y.; Shen, Y.; Wang, H.; Pan, X. Mapping the Agricultural Land Use of the North China Plain in 2002 and 2012. *J. Geogr. Sci.* **2019**, *29*, 909–921. [CrossRef]
71. Wu, X.; Qi, Y.; Shen, Y.; Yang, W.; Zhang, Y.; Kondoh, A. Change of Winter Wheat Planting Area and Its Impacts on Groundwater Depletion in the North China Plain. *J. Geogr. Sci.* **2019**, *29*, 891–908. [CrossRef]
72. Zhong, H.; Sun, L.; Fischer, G.; Tian, Z.; Liang, Z. Optimizing Regional Cropping Systems with a Dynamic Adaptation Strategy for Water Sustainable Agriculture in the Hebei Plain. *Agric. Syst.* **2019**, *173*, 94–106. [CrossRef]
73. Wen, F.; Fang, X.; Khanal, R.; An, M. The Effect of Sectoral Differentiated Water Tariff Adjustment on the Water Saving from Water Footprint Perspective: A Case Study of Henan Province in China. *J. Clean. Prod.* **2023**, *393*, 136152. [CrossRef]
74. Li, Z.; Zhou, Y.; Li, K.; Xiao, H.; Cai, Y. The Spatial Effects of City-Level Water-Energy Nexus: A Case Study of Hebei Province, China. *J. Clean. Prod.* **2021**, *310*, 127497. [CrossRef]
75. Kattel, G.; Reeves, J.; Western, A.; Zhang, W.; Jing, W.; McGowan, S.; Cuo, L.; Scales, P.; Dowling, K.; He, Q.; et al. Healthy Waterways and Ecologically Sustainable Cities in Beijing-Tianjin-Hebei Urban Agglomeration (Northern China): Challenges and Future Directions. *WIREs Water* **2021**, *8*, e1500. [CrossRef]
76. Deng, L.; Han, Z.; Pu, W.; Bao, R.; Wang, Z.; Wu, Q.; Qiao, J. Impacts of Human Activities and Climate Change on Water Storage Changes in Shandong Province, China. *Environ. Sci. Pollut. Res.* **2022**, *29*, 35365–35381. [CrossRef]
77. Xu, Y.; Gun, Z.; Zhao, J.; Chen, J.; Liu, Q.; Cheng, X.; Sutanudjaja, E.H.; Wang, J.; Liu, H.; Zhan, W. Continuing Severe Water Shortage in the Water-Receiving Area of the South-To-North Water Diversion Eastern Route Project from 2002 to 2020. *Water Resour. Res.* **2023**, *59*, e2022WR034365. [CrossRef]
78. Huang, C.; Zhang, C.; Liu, Q.; Wang, Z.; Li, H.; Liu, G. Land Reclamation and Risk Assessment in the Coastal Zone of China from 2000 to 2010. *Reg. Stud. Mar. Sci.* **2020**, *39*, 101422. [CrossRef]
79. Wang, Z.; Zhang, J.; Yang, X.; Huang, C.; Su, F.; Liu, X.; Liu, Y.; Zhang, Y. Global Mapping of the Landside Clustering of Aquaculture Ponds from Dense Time-Series 10 m Sentinel-2 Images on Google Earth Engine. *Int. J. Appl. Earth Obs. Geoinf.* **2022**, *115*, 103100. [CrossRef]
80. Su, G.; Xiong, C.; Zhang, G.; Wang, Y.; Shen, Q.; Chen, X.; An, H.; Qin, L. Coupled Processes of Groundwater Dynamics and Land Subsidence in the Context of Active Human Intervention, a Case in Tianjin, China. *Sci. Total Environ.* **2023**, *903*, 166803. [CrossRef]